Politechnika Warszawska

Wydział Fizyki

Praca inżynierska

Ocena dawki pochłoniętej metodą dozymetrii cytogenetycznej w opraciu o modelowanie Monte Carlo

Assessment of absorbed dose by cytogenetic dosimetry method using Monte Carlo modelling

Autor:
Aleksandra Powojska
nr albumu: 251 714

Opiekunowe naukowi:
mgr inż. Iwona Słonecka
prof. dr hab. Jan Pluta
dr inż. Krzysztof Fornalski

Warszawa, 2016

fizyka techniczna

Warsaw University of Technology

Faculty of Physics

Praca inżynierska

Assessment of absorbed dose by cytogenetic dosimetry method using Monte Carlo modelling

Ocena dawki pochłoniętej metodą dozymetrii cytogenetycznej w opraciu o modelowanie Monte Carlo

Author:
Aleksandra Powojska
nr albumu: 251 714

Supervisors:
mgr inż. Iwona Słonecka
prof. dr hab. Jan Pluta
dr inż. Krzysztof Fornalski

Warsaw, 2016

PHYSICS.WUT

Oświadczenie o samodzielności wykonania pracy

Politechnika Warszawska
Wydział Fizyki

Ja, niżej podpisany:

Aleksandra Powojska, nr albumu 251 714

student Wydziału Fizyki Politechniki Warszawskiej, świadomy odpowiedzialności prawnej oświadczam, że przedłożoną do obrony pracę dyplomową inżynierską pt.:

Ocena dawki pochłoniętej metodą dozymetrii cytogenetycznej w opraciu o modelowanie Monte Carlo.

wykonałem samodzielnie pod kierunkiem

mgr inż. Iwony Słoneckiej, prof. dr hab. Jan Pluta, dr inż. Krzysztof Fornalski

Jednocześnie oświadczam, że:

- praca nie narusza praw autorskich w rozumieniu ustawy z dnia 4 lutego 1994 o prawie autorskim i prawach pokrewnych, oraz dóbr osobistych chronionych prawem cywilnym,
- praca nie zawiera danych i informacji uzyskanych w sposób niezgodny z obowiązującymi przepisami,
- praca nie była wcześniej przedmiotem procedur związanych z uzyskaniem dyplomu lub tytułu zawodowego w wyższej uczelni.
- promotor pracy jest jej współtwórcą w rozumieniu ustawy z dnia 4 lutego 1994 o prawie autorskim i prawach pokrewnych

Oświadczam także, że treść pracy zapisanej na przekazanym nośniku elektronicznym jest zgodna z treścią zawartą w wydrukowanej wersji niniejszej pracy dyplomowej.

Warszawa, dnia 28 września 2016

Oświadczenie o udzieleniu Uczelni licencji do pracy

Politechnika Warszawska
Wydział Fizyki

Ja, niżej podpisany:

Aleksandra Powojska, nr albumu 251 714

student Wydziału Fizyki Politechniki Warszawskiej, niniejszym oświadczam, że zachowując moje prawa autorskie udzielam Politechnice Warszawskiej nieograniczonej w czasie, nieodpłatnej licencji wyłącznej do korzystania z przedstawionej dokumentacji pracy dyplomowej pt.

Ocena dawki pochłoniętej metodą dozymetrii cytogenetycznej w opraciu o modelowanie Monte Carlo.

w zakresie jej publicznego udostępniania i rozpowszechniania w wersji drukowanej i elektronicznej[1].

Warszawa, dnia 29 września 2016

[1]Na podstawie Ustawy z dnia 27 lipca 2005 r. Prawo o szkolnictwie wyższym (Dz.U. 2005 nr 164 poz. 1365) Art. 239. oraz Ustawy z dnia 4 lutego 1994 r. o prawie autorskim i prawach pokrewnych (Dz.U. z 2000 r. Nr 80, poz. 904, z późn. zm.) Art. 15a. „Uczelni w rozumieniu przepisów o szkolnictwie wyższym przysługuje pierwszeństwo w opublikowaniu pracy dyplomowej studenta. Jeżeli uczelnia nie opublikowała pracy dyplomowej w ciągu 6 miesięcy od jej obrony, student, który ją przygotował, może ją opublikować, chyba że praca dyplomowa jest częścią utworu zbiorowego.“

Abstract

Assessing the absorbed dose of mixed neutron-gamma radiation is a multiple step process. The total absorbed dose must be determined through either physical or biological methods of dosimetry. If neither a personal dosimeter nor a physical measurement are available, the most common biological method used is cytogenetic biodisimetry. This method requires quantifying the dicentrics found in a sample of peripheral blood from an irradiated individual. The aberration frequency is then compared to an *in vitro* dose-response curve and used to calculate the total absorbed dose. In the case of mixed neutron-gamma radiation, the cumulative dose is not sufficient. Due to how differently neutrons and gamma photons interact with matter, the separate gamma and neutron components of the absorbed dose must be determined.

The iterative method, recommended by the International Atomic Energy Agency (IAEA), is a commonly used statistical approach that accurately calculates the separate gamma and neutron absorbed doses, but only if the gamma to total absorbed dose ratio (expressed at θ) is precisely known. Bayesian statistics, on the other hand, use probability distributions to express an unknown variable, therefore when employed to assess absorbed doses of mixed radiation, they remove the need to find an exact value of θ.

The aim of this dissertation was to examine the effectiveness of an alternative statistical method for assessing absorbed doses of mixed neutron-gamma radiation. The Monte Carlo method combines the iterative and Bayesian approaches to allow the choice of using either a prior probability function or an exact value of θ for absorbed dose calculations. Additionally, the Monte Carlo technique leaves room for various statistical tests, such as a "damage time line" or the distribution of damages among cells, that can be later represented graphically.

The study involved creating a computer program implementing a Monte Carlo based algorithm and evaluating the advantages and disadvantages of the method. The results generated by the program are comparable to those acquired through methods of physical dosimetry as well as those produced by programs employing the iterative and Bayesian methods.

Keywords:

Monte Carlo statistics, biological dosimetry, mixed neutron-gamma radiation, dose assessment, chromosome aberrations, dicentrics

Streszczenie

Całkowita dawka pochłonięta przez osobę napromienioną oceniana jest metodami fizycznej lub biologicznej dozymetrii. W przypadku braku dozymetra osobistego lub gdy pomiar fizyczny jest niemożliwy, najczęściej stosuje się metodę biologicznej dozymetrii cytogenetycznej. Metoda ta polega na wyznaczeniu liczby aberracji chromosomowych (najczęściej dicentryków) w próbce krwi obwodowej i porównaniu częstości tych uszkodzeń z odpowiednimi krzywym dawka- skutek (*in vitro*) w celu ustalania pochłoniętej dawki promieniowania jonizującego. Ze względu na odmienny charakter i inne właściwości fizyczne składowych rozpatrywanego promieniowania mieszanego (promieniowania gamma i promieniowania neutronowego) niezbędnym jest ustalenie dawki pochłoniętej pochodzącej od każdej składowej.

Rekomendowana przez IAEA metoda iteracyjna to najczęściej stosowany sposób na oszacowanie tych dawek , pozwalających obliczyć wartości składowych całkowitej dawki pochłoniętej, ale jedynie wtedy, gdy stosunek dawki gamma do dawki całkowitej (oznaczany jako parametr θ) jest znany. Dokładna wartość θ nie zawsze jest dostępna. W takich sytuacjach stosuje się między innymi statystykę bayesowską, która pozwala przedstawić nieznany parametr w postaci rozkładu prawdopodobieństwa.

Celem niniejszej pracy było zbadanie skuteczność innej metody statystycznej do szacowania dawek pochłoniętych pochodzących od promieniowania mieszanego $n + \gamma$. Metoda Monte Carlo łączy podejście iteratywne z podejściem bayesowskim co pozwala na przeprowadzenie obliczeń stosując dokładną θ lub wybrany rozkład prawdopodobieństwa. Ponadto, podejście to pozwala na przeprowadzenie na zebranych danych badania statystycznego , np. historię uszkodzeń lub rozkład uszkodzeń w komórkach, których wyniki mogą być przedstawione graficznie.

W ramach pracy napisany został program komputerowy, w którym zaimplementowano algorytm Monte Carlo. Sprawdzone zostały korzyści i wady płynące z użycia tej metody. Wygenerowane przez napisany program wyniki zostały porównane z wynikami otrzymanymi metodami fizycznymi oraz tymi obliczonymi metodą iteracyjną i bayesowską.

Słowa kluczowe:

Statystyka Monte Carlo, dozymetria biologiczna, promieniowanie mieszanie neutron-gamma, ocena dawki, aberracje chromosomowe, dicentryki

Table of Contents

1 | Introduction and Purpose

There are many types of possible radiological and nuclear emergencies, ranging from major global catastrophes to work or medical related over-exposures of individuals. Regardless of the cause or magnitude of the incident, in its aftermath only one aspect matters: the health of the irradiated. The effects of ionizing radiation on the human body depend primarily on the type and dose of radiation as well as the dose rate. Some effects can be observed soon after exposure, for example skin damage or radiation sickness. These are called deterministic effects and they occur above a certain threshold dose level. Other symptoms, such as cancer or hereditary defects, can appear a long time, even years, after exposure. These are called stochastic effects. Within the standards for radiation protection, it is suggested that there is no threshold above which they occur. However, the results of research conducted in this area are not definitive.

Estimating the absorbed dose, while also keeping in mind the type of radiation, is crucial for determining whether an individual was actually exposed, as well as potentially planning treatment and providing prognostic advice. Methods of dose assessment include physical and biological dosimetry. The first of the two is based on actual measurements acquired from detection equipment, such as personal dosimeters, or the physical reconstruction of events based on the identification of the source and its location. Although personal dosimeters provide the best measurements of cumulative exposure, they have limited accuracy when dealing with incidents other than full body exposures from an outside source. In the event that physical dosimetry is not sufficient enough, the absorbed dose can be accurately assessed using biological dosimetry. Biodosimetry is the assessment of the absorbed dose based on the measurement of radiation induced biological markers in the human body, such as damaged tissues or cells. Most commonly used are the cytogenetic methods of biological dosimetry, which rely on quantifying chromosome aberrations (such as dicentrics, rings, micronuclei etc.) in lymphocytes taken from peripheral blood. Once aberration frequency is established, the absorbed dose can be calculated using coefficients from a dose-response curve. It is very important that the radiation used to create the curve corresponds as closely as possible to the radiation that is being analysed.

In some cases, acquiring the cumulative dose is not enough to properly assess the situation. This happens when mixed radiation is involved. Mixed radiation is composed of at least two types of particles. This thesis will be focusing on mixed neutron-gamma fields, produced primarily in reactors in nuclear power plants. These institutions employ many people, working on maintaining the reactor or utilizing the energy it produces. In the case of a reactor failure, they would be at risk of

being exposed to large amounts of ionizing radiation. Therefore, developing an effective method of assessing their condition is of utmost importance. It is crucial to remember that the nature of photons and neutrons is different. Because of this, the manner in which the particles interact with matter, as well as the method and degree of ionization they cause, is also very different. Treating this type of mixed exposure requires determining the ratio of one component to the other. After the quantification of a given type of chromosome aberration, statistical methods are used to estimate how much of the absorbed dose came from neutrons and how much from gamma rays. There are several such statistical methods that can be used for this, such as the iterative method or Bayesian statistics [1][2].

The goal of this thesis is to implement an alternative statistical method, the Monte Carlo technique, for assessing the absorbed dose of mixed neutron-gamma radiation based on a previously acquired dicentric frequency. The iterative method has been used for this purpose on many occasions. It is an accurate method and has proven its worth many times over. Unfortunately, it cannot be employed in cases, where the exact ratio of gamma to neutron radiation is unavailable. Bayesian statistics, on the other hand, allow for the use of probability distributions instead of exact gamma-to-neutron ratios for the same calculations. The Monte Carlo method can be employed in both situations, when the ratio is known as well as when it is not. Monte Carlo is more versatile than either of the previously mentioned methods. It collects data in such a way that allows for statistical analysis of the virtually irradiated cells [2]. If needed, the distribution of neutron- and gamma-induced damages among the cells can be examined [1].

This thesis aims to apply this method and evaluate its advantages and limitations in order to assess whether it is an appropriate replacement for the iterative and Bayesian methods. As part of this paper, the Monte Carlo technique is to be implemented within a specialized computer program consisting of a user-friendly graphic interface and presenting results both numerically and visually.

2 | Theory

2.1 Ionizing radiation

2.1.1 Introduction

Radiation is the transmission of energy through space or a material medium in the form of particles or electromagnetic waves. Depending on its level of energy as well as its interactions with matter, radiation can be categorized as either non-ionizing or ionizing. The term ionizing describes radiation that has a sufficient amount of energy to free electrons from atoms or molecules. It is produced during nuclear reactions, nuclear decay, through the acceleration of charged particles or in very high temperatures. Natural sources include the Sun, supernova explosions and natural radioisotopes. Some artificial sources are nuclear reactors, particle accelerators and x-ray tubes. There are different types of ionizing radiation that can be categorized based on the nature of the particles or waves that cause the ionization. Each has a different ionization mechanism that can be described as either direct or indirect [3]. Directly ionizing radiation, such as alpha or beta radiation, is usually caused by the flow of charged particles, creating the direct ionization and excitation of atoms through coulombic interactions. Indirectly ionizing radiation, for example gamma or neutron rays, is caused by particles with no charge. The ionization effects are caused mainly by secondary ionizations. This section will discuss a few fundamental types of ionizing radiation and how they affect the human body.

2.1.2 Types of ionizing radiation

Alpha particles, created when atoms undergo radioactive decay, are composed of two neutrons and two protons. They are usually emitted by heavy radioactive nuclei and their energies range from 4 to 9 MeV [4]. Because of their large mass and electric charge, they react strongly with matter, causing numerous instances of excitation and ionization per unit of length. As a consequence, alpha particles quickly lose their energy and have a very short range of no more than a few centimetres in air. Nevertheless, it is possible to accelerate alpha particles to energies that allow them to travel even through several centimetres of lead. Alpha particles ionize matter directly. When passing through a material medium, whether it be tissue or air, the particles ionize atoms by causing the detachment of their outer orbital electrons. Each time this happens, these particles lose energy and slow down. The relationship between a particle's energy loss and the distance that is has travelled

is illustrated by the Bethe-Bloch formula [5]:

$$-\frac{dE}{dx} = Kz^2\frac{Z}{A}\frac{1}{\beta^2}\left(\frac{1}{2}\ln\frac{2m_e c^2\beta^2\gamma^2 T_{max}}{I^2} - \beta^2\right) \tag{2.1.1}$$

where

dE/dx - amount of energy lost by a particle per unit of track length

K - combination of several constants (K = 307 keVcm^2/g)

z - incident particle charge

Z, A - atomic number and mass number of the medium

β - particle speed ($\beta = v/c$)

m_e - electron mass

c - speed of light

I - mean excitation potential:

$$I = 9.1 \cdot Z\left(1 + \frac{1.9}{Z^{2/3}}\right)\text{eV} \tag{2.1.2}$$

T_{max} - maximum energy that can be transferred to an electron through a single collision:

$$T_{max} = \frac{2m_e c^2\beta^2\gamma^2}{1 + 2\gamma\frac{m_e}{M} + \left(\frac{m_e}{M}\right)^2} \tag{2.1.3}$$

M - particle mass

γ - relativistic factor:

$$\gamma = \frac{1}{\sqrt{1-\beta^2}} \tag{2.1.4}$$

Energy loss per unit of length is inversely proportional to the square of particle speed ($1/\beta^2$). This means that as the speed of the particle decreases, the energy loss per unit or track length begins to increase rapidly. The slower the alpha particles travel, the more time they have to interact with atoms, increasing the chance of ionization. Once they come to a complete stop, they collect two electrons and become helium atoms. Although alpha radiation is not suitable for radiation therapy, they can be very destructive when ingested. Within their short range, they can be more dangerous than most types of radiation.

Beta radiation takes the form of high-speed electrons or positrons. Beta particles are smaller and lighter than alpha particles, therefore they are able to travel farther, up to a couple of meters in air, depending on their energy. They can penetrate a few centimetres of skin, but similarly to alpha radiation, the main threat comes from ingesting beta-emitting material. Although the emission of beta particles can be induced by many things, only the most important ones with regard to biological effects will be discussed. One type of radioactive decay where beta

rays are released is called beta decay. There are two forms of beta decay: electron emission (β- decay) and positron emission (β+ decay). The first can occur when an atom with an excess of neutrons is attempting to reach a more stable state. During the process of β- decay, a neutron is converted into a proton, electron and electron antineutrino. Positron decay is the conversion of a proton into a neutron, positron and electron neutrino. This type of decay may happen in atoms with an excess of protons. These types of beta radiation ionize matter directly. Because of their negative charge, β- particles interact with the orbital electrons of atoms, causing excitation or ejecting them from their orbits, resulting in the ionization of the atoms. Positively charged β+ particles interact similarly with matter when they have a sufficient amount of energy. Once they stop, they combine with an electron causing the annihilation of the pair and the emission of two gamma rays. A mechanism that can be considered equivalent to proton emission is electron capture. Electron capture is occasionally classified as a type of beta decay. The nucleus of an unstable atom attracts an electron from an inner orbit. It is then combined with a proton to create a neutron. The vacancy on the orbit is then filled by an electron from an outer shell. This transition causes the emission of a gamma ray.

Gamma decay is a form electromagnetic radiation, consisting of high-energy photons being released from unstable atoms transitioning towards a more stable state. Gamma radiation is very penetrating, it can travel long distances in air and easily pass through the human body. Lead is an effective gamma-shielding material because of its density and large number of electrons, which absorb and scatter the energy of the radiation. As mentioned in the previous paragraph, gamma rays often follow the emission of beta or alpha radiation. They can also be emitted by natural radioisotopes. Gamma particles can ionize matter through the photoelectric effect, the Compton effect and positron-electron pair production. The photoelectric effect describes a process during which a photon transfers all of its energy to an atomic electron, causing it to eject from the atom. The vacancy left in one of the atom's shells is promptly filled by an electron from a shell with a lower binding energy, which results in the release of an X-ray photon. This effect is the dominant ionization mechanism for photon energies below 50 keV. It becomes less significant as the energy increases. Compton scattering occurs when a photon interacts with an atomic electron in such a way that part of its energy is transferred to the electron, causing its ejection, while the rest of the energy is released as a lower energy photon. This effect is the primary ionization mechanism for intermediate energies. Positron-electron pair production becomes most significant for energies over 5 MeV. It is the interaction of a photon with the electric field of a nucleus, resulting in the conversion of the photon to an electron and positron. This process can only occur for photon energies above 1.02 MeV (the rest mass of two electrons). Although the above effects

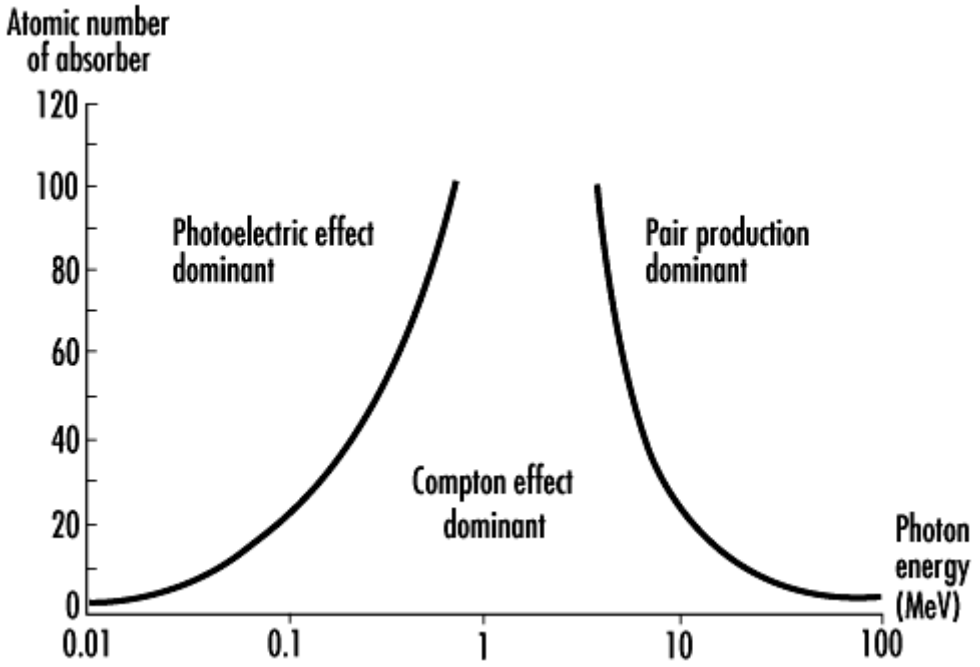

Figure 2.1.1: An illustration of relative importance of the three gamma ionization mechanisms [6]

allow gamma rays to ionize matter directly, the secondary electrons or positrons that are produced in these processes have enough energy to cause many more instances of ionization, therefore the indirect (secondary) ionization is more prominent.

Neutron radiation is a type of particle radiation consisting of free neutrons, usually released during spontaneous or induced nuclear fission (for example in nuclear reactors). Unlike the previously discussed types of radiation, neutrons are neutral particles which allows them to travel thousands of meters without any incidents and making them much more penetrating than alpha or beta rays (in some cases even gamma rays). They aren't affected by either the electrons that orbit atoms or the electric field created by the positively charged nucleus. These particles travel in straight lines, only swerving from their tracks when they collide with a nucleus [3]. Due to the lack of any electric charge, neutrons cannot directly ionize matter. Neutron radiation interacts with matter through several kinds of mechanisms (as shown in Figure 2), that can be categorized as one of two major types: scattering or absorption. The scattering of a neutron on a nucleus can be either elastic or inelastic. The first describes a collision during which a part of the neutron's energy is transferred to the nucleus, but no energy is emitted, therefore the cumulative energy of the neutron and nucleus stays the same. Inelastic scattering is similar, however it can only occur if the incident energy of the neutron is enough to put the target atom into an excited state and causing it to eventually release excess energy in the form of radiation. A neutron may also be absorbed or captured by a nucleus, resulting in several forms of emission. The internal structure of the nucleus may be rearranged causing it to release one or more gamma photons. The

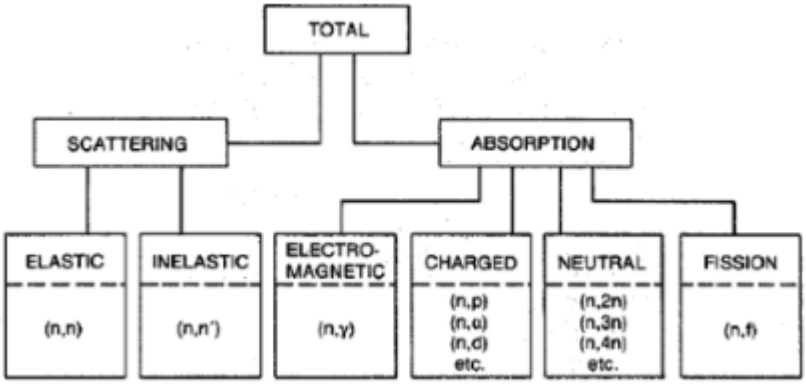

Figure 2.1.2: Categories of neutron interactions. The letters separated by commas in the parentheses represent the incoming and outgoing particles.

emission of charged particles, most commonly protons, deuterons or alpha particles, is also possible. Alternatively, the nucleus may also release excess neutrons. If only one neutron is released, the interaction is indistinguishable from scattering. A fission event may also occur, resulting in two or more fission fragments and extra neutrons [7]. Unlike in the case of gamma radiation, materials with a high atomic mass number, such as lead, are not effective shields for this type of radiation. Neutrons must be attenuated and slowed to thermal energies by elastic collisions and subsequently absorbed by the nuclei of the shield material. The average energy loss of a neutron with a kinetic energy of E colliding with a nucleus with a mass number A is $2EA/(A+1)^2$. In order to achieve the maximum energy loss with the fewest number of elastic collisions, the mass number of the target nuclei should be as small as possible. Hydrogen-rich materials, such as water or paraffin, are effective neutron shields. Hydrogen has no excited states, therefore inelastic scattering is impossible. It has a mass number equal to 1, so the energy loss during a neutron-hydrogen collision is at its largest possible value of E/2. [7][8]

With the advancement of technology, our ability to harness nuclear energy for a variety of purposes is increasing. In many facilities and institutions, the presence of mixed radiation fields is very common. Mixed radiation is a combination of at least two different types of particles. This thesis focuses on a specific type of mixed field i.e. neutron-gamma radiation. Most neutron-gamma fields originate from reactions or isotopes used in nuclear reactors. Although the majority of these isotopes release a gamma dominated n+γ field, gamma-neutron proportions may vary [9]. The ratio of one component to the other depends on the source. The reactors produce energy through nuclear fission, the splitting of a heavier atom into two lighter atoms. The target nucleus absorbs a neutron, causing it to break apart, simultaneously releasing kinetic energy, gamma photons and free neutrons. Nuclear reactors can serve many purposes, such as producing electricity or isotopes for medical or industrial use [10]. Because of the versatility of this technology, nuclear power plants can employ

hundreds of workers. These are the people who would be in danger of being heavily exposed to ionizing radiation during a nuclear reactor failure or malfunction, which is why it is important to find a fast and accurate method of neutron-gamma dose assessment.

2.1.3 The effect of radiation on the human body

The amount and type of ionization incidents left by a particle travelling through a medium depends on the type of radiation, its energy as well as the route of exposure (such as external, internal or skin contamination). The first two can be expressed as one factor, called the LET (linear energy transfer) coefficient. LET, expressed in MeV/μm, describes the amount of energy transferred to the medium per unit length of travel in the form of ionization or excitation. Alpha particles and neutrons have a relatively high LET coefficient, while gamma and beta particles have a lower LET coefficient. What this means is that a certain amount of neutrons passing through matter will create more ionization or excitation incidents than the same amount of gamma photons. The linear energy transfer value can aid in estimating the potential for biological damage from different types of radiation. As shown in Figure 2.1.3, low LET radiation creates ionizations that are randomly

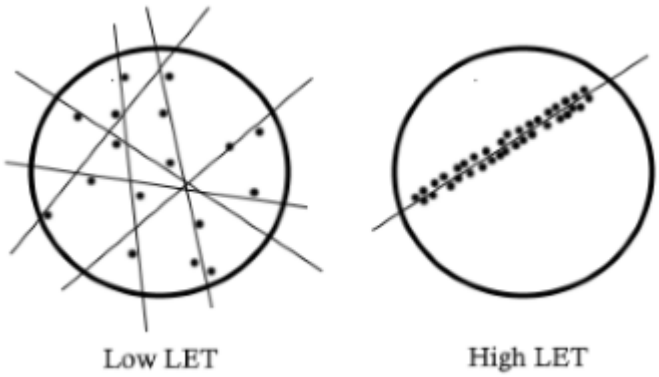

Figure 2.1.3: Low and high LET

distributed among a very large number of tracks, while with high LET radiation there are fewer tracks and energy is deposited in "discrete packets" [11].

In Poland, the average effective dose per individual is 3,5 mSv/year, 74% of that comes from natural sources (the rest comes from artificial sources, primarily in the form of medical radiation) [13]. Over time, the human organism has developed highly efficient methods to deal with the effects of background radiation coming from all around us. The repair of strand breaks and other damages to the DNA is a natural procedure that is usually accurate. Figure 2.1.4 illustrates the process. The numbers in parentheses represent fractions of metabolic DNA damage from low-LET background radiation (0.1 cGy/year) DNA damage [12]. (more about figure.)

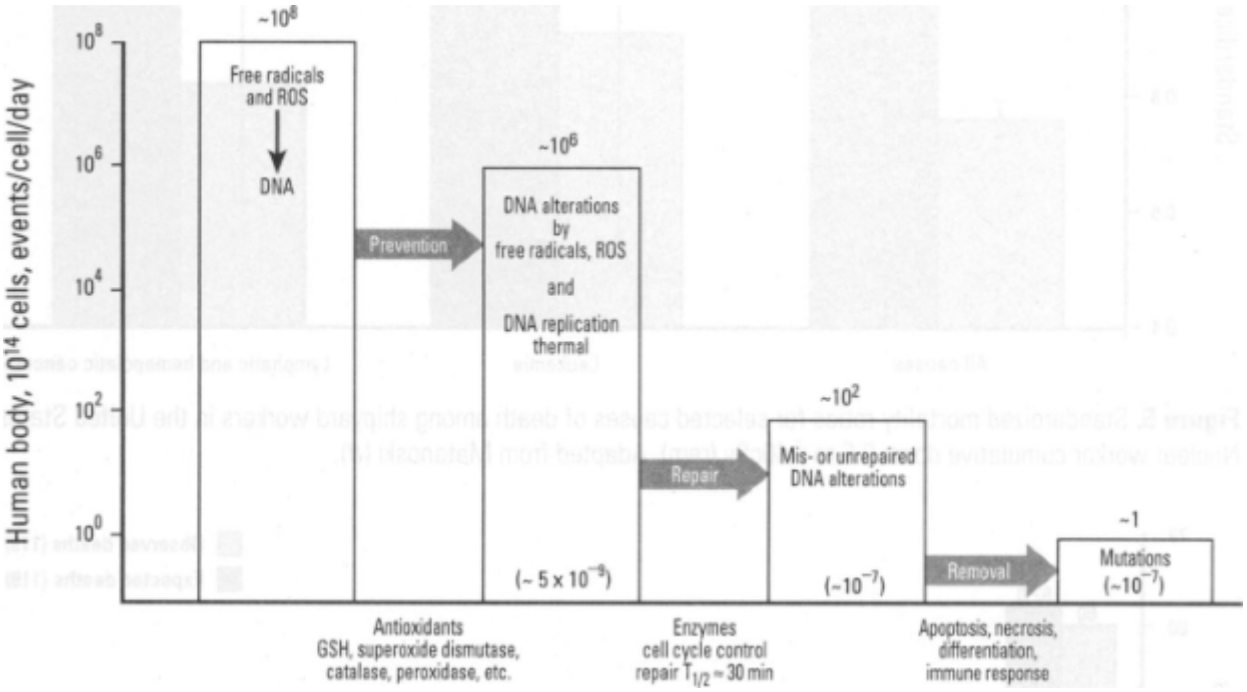

Figure 2.1.4: DNA damage control and repair system. GSH: glutathione redustase (enzyme). ROS: reactive oxygen species [12]

Both low and high LET radiation can cause a variety of damages to the DNA, as illustrated in Figure 2.1.5. The types of harmful alterations include base damage (BD), abasic sites (AS), DNA protein cross-links (DPC), single strand breaks (SSB) as well as double strand breaks (DSB) [11][14].

Individual BD, AS and SSB are non-complex changes that can be repaired by processes such as base excision repair (BER), nucleotide excision repair (NER) or single strand break repair (SSBR). DPC can be fixed through the NER mechanism or the homologous recombination repair (HRR). DSB are more difficult to rectify, they are critical damages that are responsible for most of the radiation-induced mutations. Two important DSB repair mechanisms are the HRR and DNA non-homologous end-joining (NHEJ). Higher doses of radiation may also cause clusters of DNA lesions, or Multiple Damage Sites (MDS), that can become increasingly difficult to repair. [11][14]

Although, as mentioned before, the human body has the ability to deal with a certain amount of irradiation, high doses of ionizing radiation can increase the probability of double strand breaks as well as clusters of various DNA lesions and cause permanent damage. Studies on radiation track structure show that low-LET radiation can create smaller, localized clusters of excitations and ionizations within a single electron-track, while the clusters caused by high-LET radiation are more numerous and larger in a spacial extent [11][15].

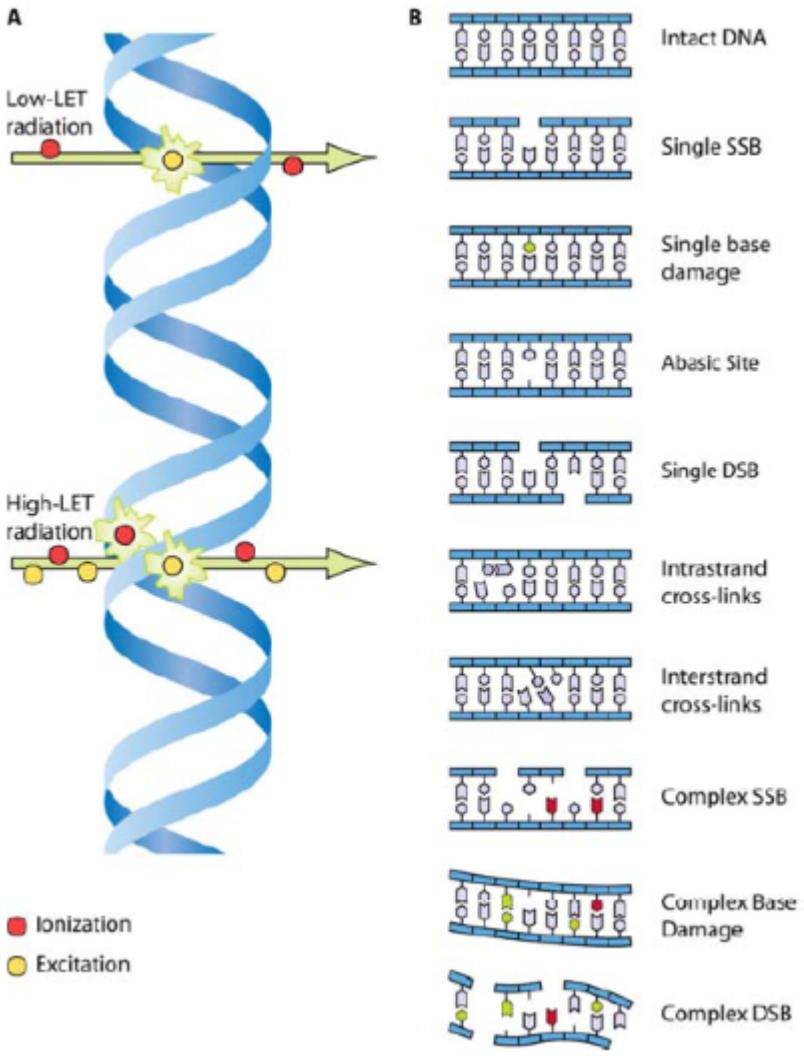

Figure 2.1.5: **A**: Ionization pattern for low and high LET radiation. **B**: Radiation induced lesions in the DNA

2.1.4 Types of chromosome mutations

There is a wide variety of mutations that are caused when the repair of radiation-induced DNA lesions does not occur or when it is done improperly or incompletely.

Dicentrics, centric rings, acentrics

Dicentrics are chromosomes that have two centromeres[1] instead of one. They occur when two chromosomes have been broken in close proximity to one another and their centromeric sections attach to each other. With higher doses of radiation there are more breaks of the DNA, therefore the probability of multicentric configurations rises. Tricentrics, quadricentrics etc. are also possible [14]. Centric rings are

[1] A centromere is the central region of the chromosome, where two chromatids are held together.

much less common than dicentrics. They occur when both or one of the chromosome ends have been lost, allowing the fusion of its arms. During dose estimation, some scientists combine the centric ring count with the dicentric count, while others choose to completely ignore them [11]. Acentrics, chromosome fragments that lack a centromere, often occur alongside dicentric or centric ring formation, although they can also form independently. Acentrics can be created through interstitial deletions, caused by two DNA breaks, or through terminal deletion, caused by one break.

The mutations discussed above are classified as unstable chromosome aberrations. They can cause a mitotic catastrophe, which is the death of a cell during mitosis, the part of the cell cycle when a single cell divides to create two identical cells. This occurs when a cell enters mitosis with incompletely or incorrectly repaired DNA strands, causing the loss of genetic material or making its replication and separation impossible, resulting in a decline in the amount of these types of aberrations with each cell division cycles (with a half-life of about 130 days). Dicentrics occur spontaneously around once per 1000 cells [16][17][18].

Translocations

A translocation is the rearrangement of parts within a chromosome or between chromosomes. Intrachromosomal translocations are relocations of a chromosome fragment within the chromosome.These movements are usually non-reciprocal, meaning that a different chromosome part does not take the place of the rearranged one. Interchromosomal translocations occur between two chromosomes. They can be either reciprocal, where a segment from one chromosome exchanges places with a segment from another chromosome, or non-reciprocal, where the exchange is one-way [19].

Translocations are stable mutations. Chromosomal material, while being in a different order after the translocation, is still maintained. Because of this, they do not cause cell death during division, meaning that they can be passed on to future generations of cells. Because of this, the translocation count does not change drastically with time and an accurate dose assessment is possible even years after exposure. Translocations occur spontaneously in 4-12/1000 cells [20].

Micronuclei

Micronuclei(MN) are formed when an acentric fragment, or an entire chromosome that has been malsegregated during mitosis, is not included in the daughter nucleus. These excluded chromosomes or fragments become enveloped by a nuclear membrane, creating a small extra nucleus, a micronucleus that is morphologically similar to its standard-sized counterpart. MN have a relatively high and variable spontaneous frequency (2-36 MN/1000 cells) that is influenced by age, gender as

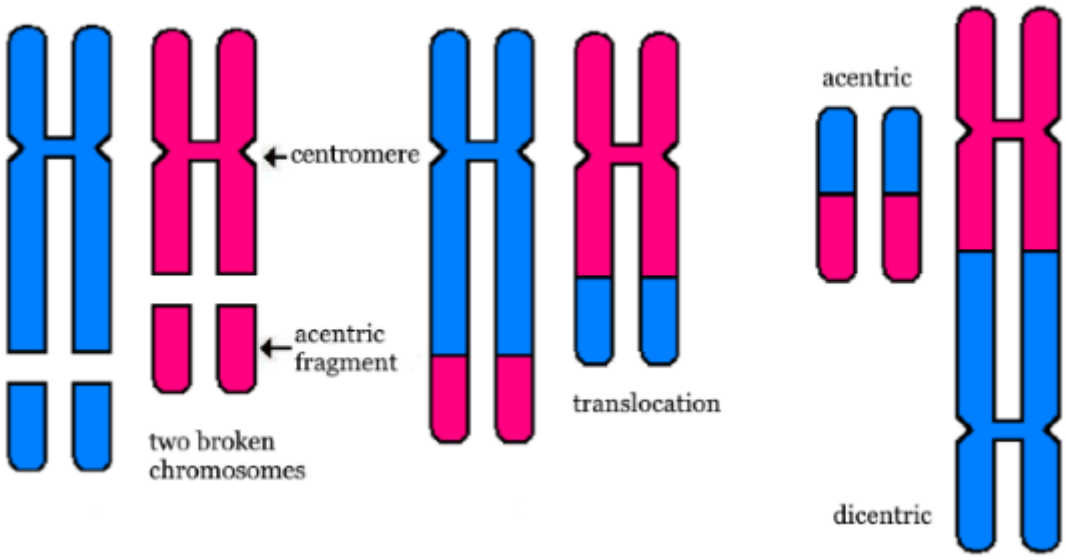

Figure 2.1.6: The difference between a dicentric and a translocation [20]

well as smoking [21].

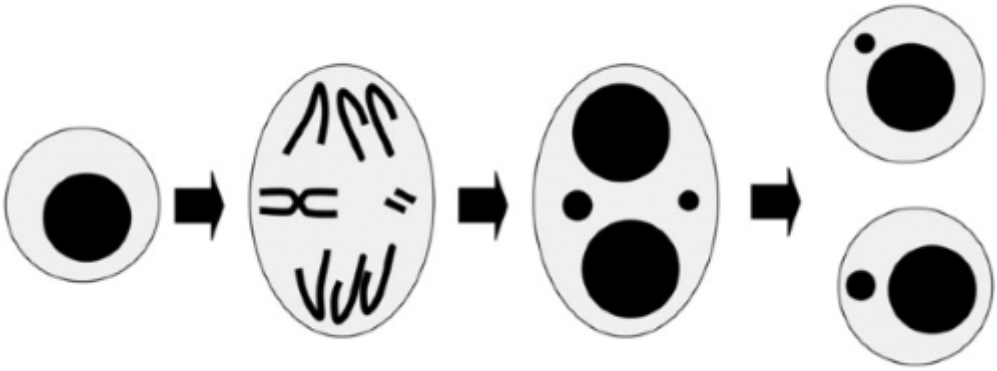

Figure 2.1.7: Micronucleus formation caused by chromosome loss or break [22]

The number of dicentrics, translocations and micronuclei depends on the absorbed dose, which is why they can be used as biological markers for radiation dose assessment. This topic will be discussed further in the section 2.2.

2.1.5 Radiation health effects

The human DNA damage-repair system cannot deal with excessive amounts of damages. If an alteration is too severe and cannot be repaired, the cell will either die or mutate. If cells die more rapidly than the organism is able to produce new cells, *deterministic* health effects will begin to appear. The dose that causes too many cells to die is called the threshold dose and it is specific to particular tissues. Deterministic effects usually appear soon after irradiation. They gained their name because their intensity is determined by the type and dose of radiation.

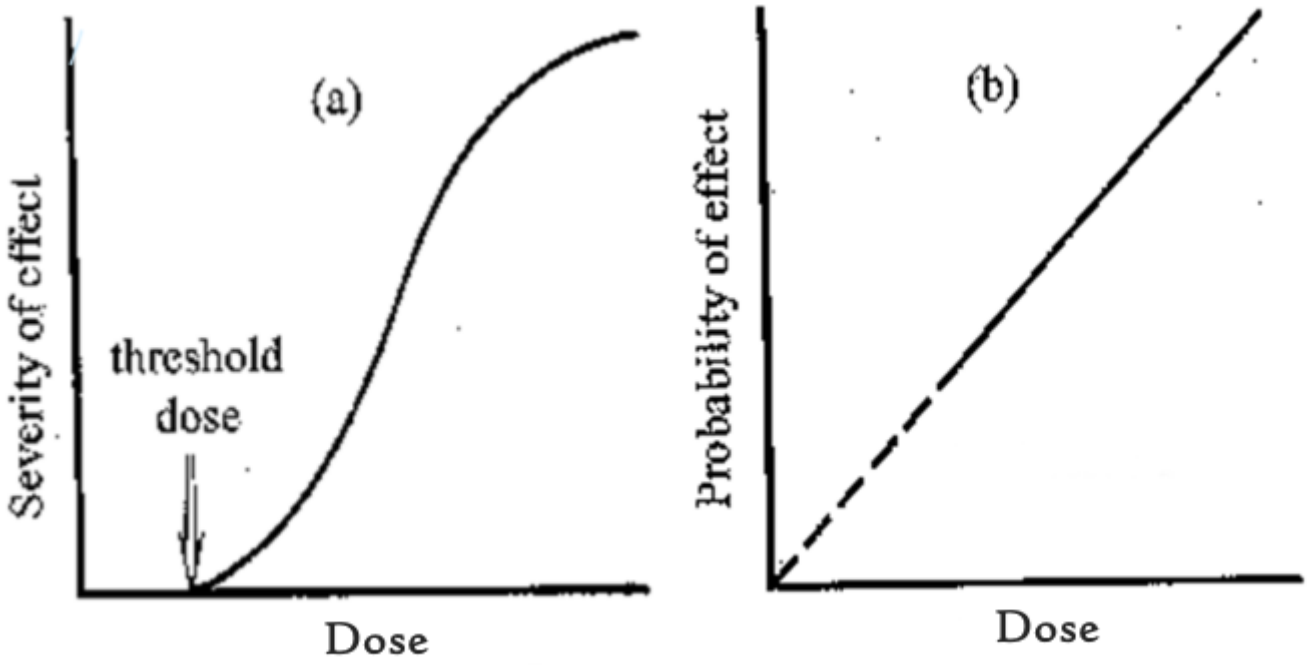

Figure 2.1.8: (a) The severity of deterministic effects based in the dose; (b) the probability of stochastic effects based in the dose (with a linear assumption in the low dose region) [26]

They include irreversible skin damage, hair loss, sterility, nausea and vomiting. If the damage is repaired inaccurately or incompletely, cells may develop mutations, such as chromosomal aberrations. Even though these mutations may not cause immediate health problems, they can result in serious future health issues, such as cancer or hereditary defects. Delayed effects such as these are *stochastic* effects. The severity of these effects is independent of the dose, but within the standards of radiological protection, it is accepted that the probability of them occurring if proportional to the absorbed dose [23][24][25].

Figure 2.1.8(a) shows the relationship between absorbed dose (in Gy) and the severity of deterministic health effects. Before the threshold dose, these effects do not occur. Figure 2.1.8(b) is the relationship between the dose (in Sv) and the probability of the onset of stochastic effects. According to the linear nonthreshold hypothesis (LNT), there is no threshold dose for stochastic effects and they can occur even at small doses [25]. The shape of this dose-reponse curve has been the topic of immense debate for many years. According to the National Council on Radiation Protection and Measurements (NCRP) Report 121, the LNT hypothesis is accepted based on knowledge of the basic mechanisms that cause stochastic effects and the biophysical concept that any single charged particle passing through a cell can damage the DNA and ultimately lead to cancer. There is biological data that contradicts the LNT, such as increased lifespan and a decrease of cancer rates in areas with a high background radiation level (for example Misasa, Japan where there

are radon spas). More information on the subject can be found in [27].

2.2 Biological dosimetry

2.2.1 Introduction

Dosimetry is a branch in the field of nuclear physics that deals with measuring and assessing ionizing radiation doses. Although there are several types of dosimetry, this section will discuss biological dosimetry, which refers to the use of biological matter from irradiated individuals to estimate the dose of radiation they received.

2.2.2 Concepts and quantities

When assessing a potential biological response to ionizing radiation, the most important dosimetric quantity to consider is the *absorbed dose* (D). Absorbed dose (measured in grays: 1 Gy = 1 $\frac{J}{kg}$) is defined as the amount of energy deposited into a medium per unit of mass [17]:

$$D = \frac{dE}{dm} \tag{2.2.1}$$

Absorbed dose is used for all types of media and particles, however it has limitations. Most importantly, depending on the LET, the same dose of various types of radiation can produce severely different biological responses. It is also limited by the fact that energy deposition differs from one variety of living tissue to another. Before 1990, in order to take these differences into account, a quality factor, Q, was applied to the absorbed dose. In 1990, for the purpose of radiation protection, the International Commission of Radiological Protection (ICRP) recommended using a completely different quantity to express dose with regard to the type of radiation as well as the affected tissue [28]. This quantity, measured in sieverts (Sv = 1 $\frac{J}{kg}$ = 1 Gy [2]), is called the *equivalent dose* (H_T):

$$H_T = \sum_R w_R D_{T,R} \tag{2.2.2}$$

where w_R is the weighting factor for radiation type **R** (see Table 1 below) and $D_{T,R}$ is the absorbed dose of radiation **R** in tissue **T**.

Both Q and w_R are based on a value called the *relative biological effectiveness* (RBE), which allows for the contrast between biological effectiveness and different forms of ionizing radiation. According to the International Atomic Energy Agency

[2] Gray is a physical quantity, sievert is a biological quantity. From [29]: "1 mSv is the dose produced by exposure to 1 milligray (mG) of radiation."

(IAEA), RBE is defined as "the ratio of the dose of the reference radiation (usually, orthovoltage X rays) to the dose of the particular radiation being studied that produces the same biological effect" [11].

Table 2.2.1: Radiation weighting factors [28]

Radiation type & energy range	$\mathbf{w_R}$
X/γ rays, all energies	1
Electron, positrons, muons, all energies	1
Neutrons:	
$<$ 10 keV	5
10-100 keV	10
$>$ 100 keV to 2 MeV	20
$>$ 2 MeV to 20 MeV	10
$>$ 20 MeV	5
Protons (except recoil protons), $>$ 2 MeV	2-5
α particle, heavy nuclei, fission fragments	20

The weighting factors above are valid internationally, although the ICRP published a new set of values in 2007 that can be found in ICRP Publ. 103: The 2007 Recommendations of the International Commission on Radiological Protection.

In order to acknowledge every irradiated tissue or organ adding to the cumulative health effects, another concept, called the *effective dose* (E), was introduced:

$$E = \sum_T w_T H_T \tag{2.2.3}$$

where w_T is the tissue weighting factor, representing the relative contribution of tissue **T** to the cumulative damage done by the uniform irradiation of the whole body [17].

Table 2.2.2: Weighting factors for specific tissues from (ICRP 1991) and (ICRP 2007)

Type of tissue	$\mathbf{w_T(1991)}$	$\mathbf{w_T(2007)}$
Gonads	0.20	0.08
Red bone marrow	0.12	0.12
Colon	0.12	0.12
Lung	0.12	0.12
Stomach	0.12	0.12
Bladder	0.05	0.04
Breast	0.05	0.12
Liver	0.05	0.04
Oesophagus	0.05	0.04
Thyroid	0.05	0.04
Skin	0.01	0.01
Bone surface	0.01	0.01
Remainder	0.05	0.12

2.2.3 Cytogenetic biodosimstry

Biological dosimetry is composed of a series of methods that use radiation-induced biological changes such as bioindicators (which can be found in hematological, gastrointestinal, cerebrovascular and cutaneous systems), radiation biomarkers (chromosome aberrations), as well as other available biodosimetric techniques or procedures to assess the level of radiation absorbed by an individual [30]. Out of all the available approaches, cytogenetic analysis has become the most prevalent and frequently used method [31]. The basis of cytogenetic biodosimetry is the study of chromosome irregularities within cells, more specifically, lymphocytes taken from peripheral blood. Blood samples are easily obtained, stored and transported. These particular cells are used mainly because they circulate throughout the entire body making it possible to estimate the absorbed dose even in the event of partial body exposure. Cells found in the peripheral blood are predominantly in the inactive G_0 phase of the cell cycle. No more than 0.2% of the cells are in the autosynthetic cell cycle [11]. Cytogenetic biodosimetry provides several types chromosome aberration analyses that can be used to estimate the number of chromosome irregularities. No single assay can be applied to all possible radiation scenarios. Although this thesis focuses on the dicentric assay, other methods will also be discussed.

In order to properly identify the shape and size of individual chromosomes, the cell must begin mitosis, which is when chromatin condenses into chromosomes. Artificial *in vitro* stimulation of the cell culture into mitosis is possible using a

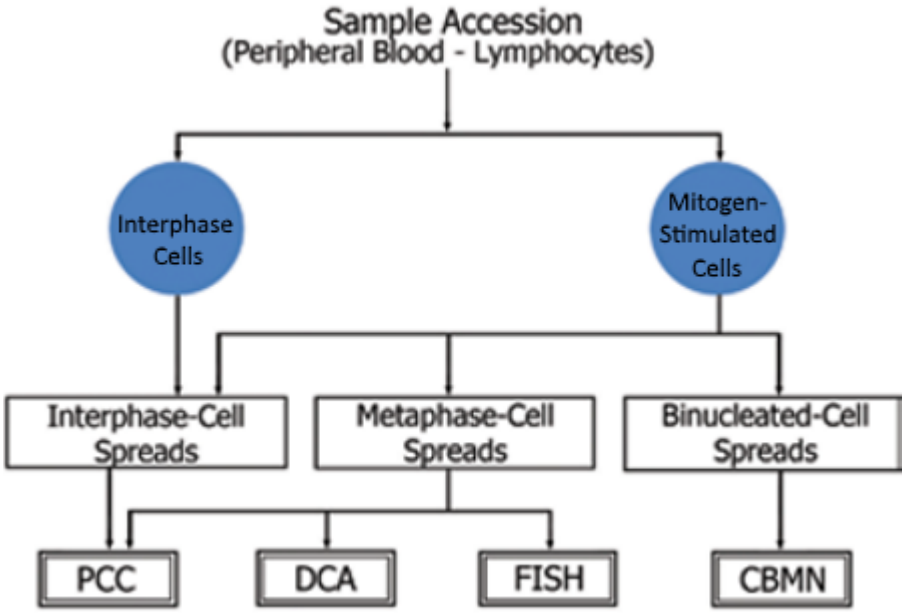

Figure 2.2.1: Various aberration assays used to assess absorbed doses [30].

mitogen called phytohaemagglutinin (PHA). Lymphocyte cultures are typically incubated for 48 hours, although culturing times may vary from 46 to 52 hours [14][20]. Once the cells begin to enter metaphase, the cycle can be stopped with the use of an alkaloid compound called Colcemid. To enable scoring, the samples must be stained accordingly, with either Giemsa or FISH (fluorescence *in situ* hybridization) [11][32].

DCA

Although standard Giemsa staining is mainly used to evaluate several kinds of unstable chromosome aberrations (i.e. dicentrics, centric rings and acentrics fragments), in the context of biological dosimetry, dicentric assays are the preferred method of analysis. The main reason for this is the low background level of dicentrics (0.5-1/1000 cells) and the reliability of detection. Metaphase-spread dicentric chromosome aberration assays (DCA) are usually employed in the earlier stages after irradiation.

Figure 2.2.2 shows standard Giemsa staining on the left and Giemsa staining using the C-banding method (selective staining of centromeres) on the right. A significant disadvantage of this method is the instability of the aberrations. Damaged cells disappear from circulating peripheral blood and are replaced by new cells at an exponential rate[11][18]:

$$N = N_0 e^{-t/t_0} \tag{2.2.4}$$

where N_0 is the starting number of cells with a dicentric and t_0 is the half-life of these cells, estimated to be approximately 130 days (between 95 and 220 days).

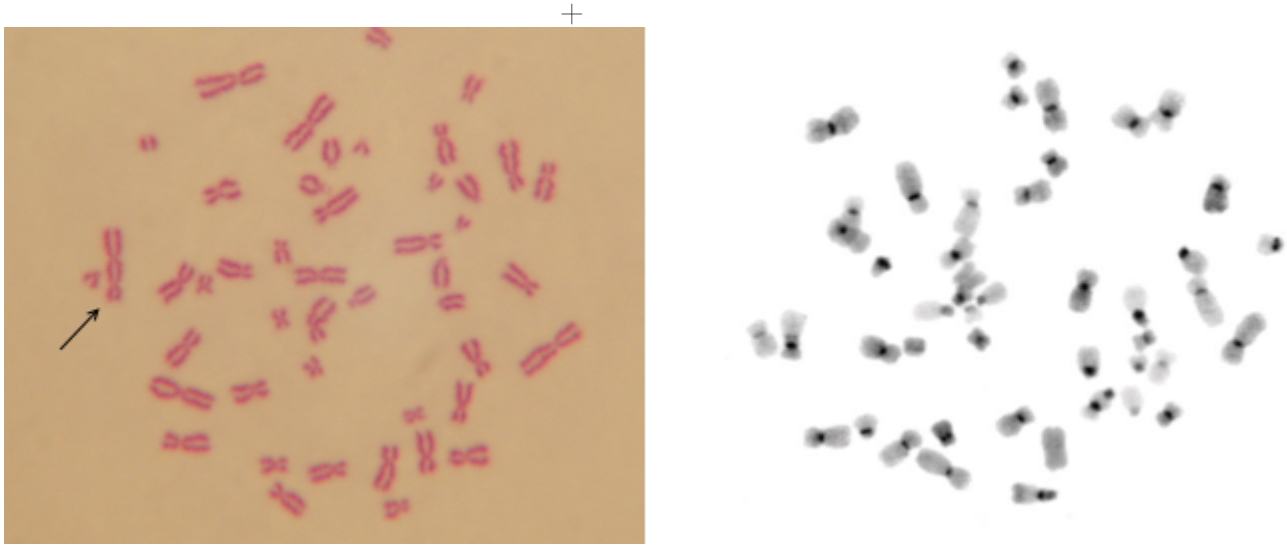

Figure 2.2.2: Pictures of dicentric chromosomes after staining [20].

FISH

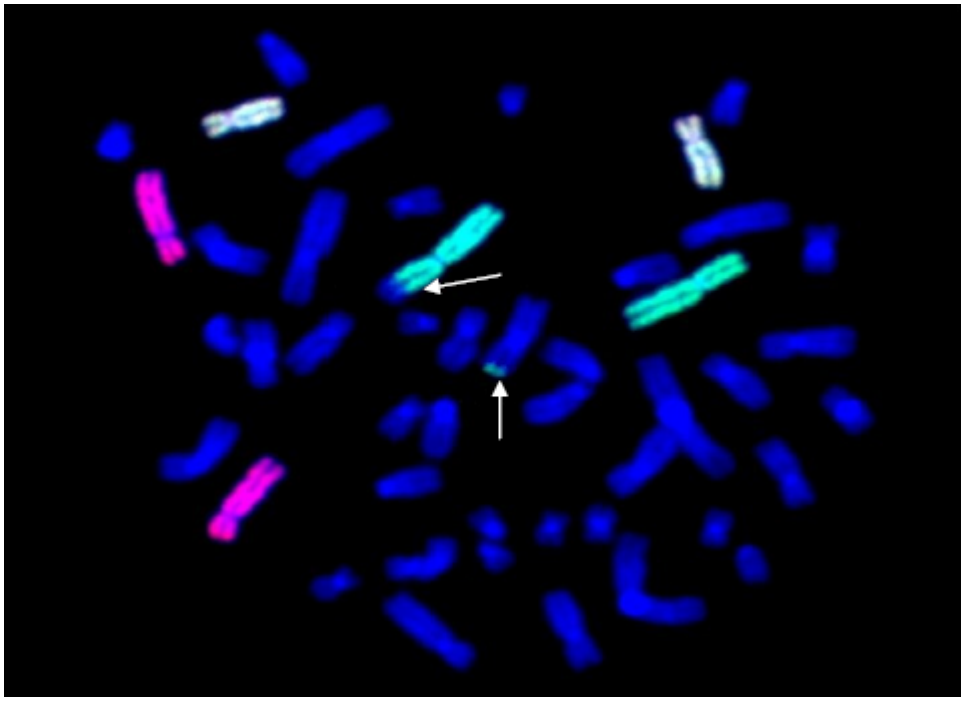

Figure 2.2.3: Highlighted chromosomes with translocations [11].

Metaphase-spread fluorescence *in situ* hybridization (FISH) translocation assays can be employed in scenarios where a dicentric assay would prove ineffective, even years after exposure. The stability of translocations allows for the analysis of old or long-term exposures. The aim of this technique is to identify certain parts of the genome by using complementary nucleotide sequences as probes and highlighting the region of interest with different colours by attaching fluorochromes [14]. Compared to dicentric scoring, which is very time-consuming and must be done by

an expert, scoring FISH-stained translocations is simpler and requires less time (although it is still relatively time consuming) [31][16]. A major disadvantage of this assay is its cost.

PCC

With accidental exposures over 6 Gy, standard *in vitro* mitosis stimulation may prove ineffective due to lymphopaenia, mitotic delay and cell death during culture, leading to a significant underestimation of the absorbed dose. Premature chromosome condensation (PCC) assays are techniques that induce chromatin to condense before the first mitosis, which causes the reduction or complete omission of culture incubation time. Premature condensation can be achieved through mitotic fusion or chemical induction. The first of the two is the fusion of cells in interphase with Chinese hamster ovary (CHO) mitotic cells by means of the fusing agent polyethylene glycol (PEG). Chemical induction consists of the rapid interphase chromosome assay (RICA) and the ring assay. Both mitotic fusion and RICA eliminate the long incubation period. The PCC ring assay, while it does require culturing, can be used for extreme overexposures. Any PCC procedure can be followed by Giemsa or FISH staining. Overall, this set analysis techniques is most useful when dealing with high doses or partial body exposures [11][33].

CBMN

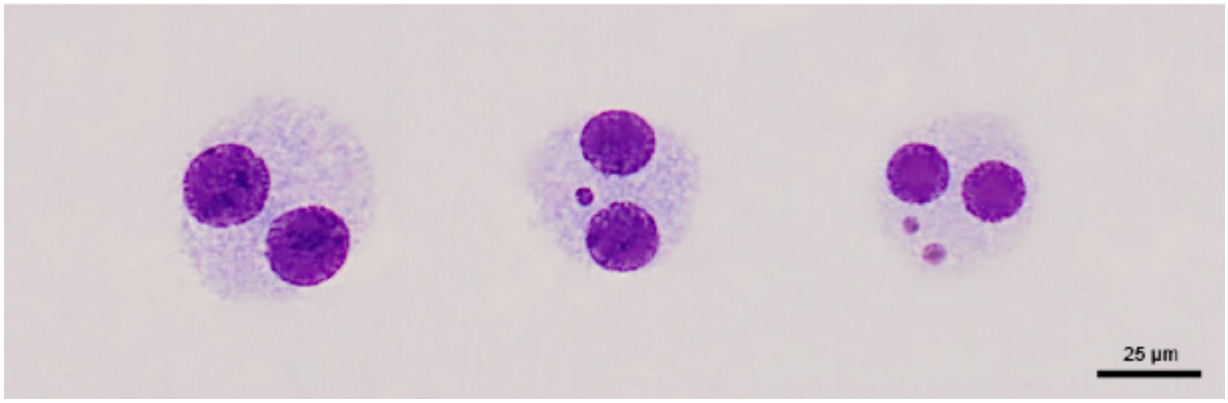

Figure 2.2.4: Giemsa stained cells without and with 1 and 2 micronuclei[11]

The formation of micronuclei is caused by chromosome aberrations, therefore they can be considered an indirect measure of chromosome damage. The cytokinesis block micronucleus (CBMN) assay requires cell culturing similar to that of the dicentric assay, but with a few differences: (i) the culture time is 72 hours, (ii) Colcemid is not used for stopping the cell cycle, (iii) cytochalasin-B is added to the culture to block cytokinesis (the process during which the cytoplasm of a single cell is divided into two), therefore allowing for the production of binucleate cells instead

of two daughter cells. Hypnotic treatment, fixation and centrifugation are also modified in order to keep the cytoplasm intact. The cells can be subsequently stained with either Giemsa or FISH for manual scoring or with DAPI(4',6-diamidino-2-phenylindole) for automated analysis. A significant advantage of CBMN is that the scoring of micronuclei does not require highly trained and experienced personnel. It is also must faster, which is important when dealing with large scale radiation incidents where a rapid biological dosimetry assay is needed. An important drawback of this method is it's unreliability in assessing low doses (below 0.2-0.3 for γ-rays or X-rays) because of its high background frequency [11][31].

Dose-response curves

In order to estimate the absorbed dose, the chromosome mutation score must be interpreted using a reference dose-response calibration curve. The International Atomic Energy Agency recommends that any laboratory that intends to employ biodosimetric methods of absorbed dose assessment should produce its own *in vitro* calibration curve. The employment of a dose-response curve established elsewhere may create extra uncertainties and cause misinterpretations[11][14]. When dealing

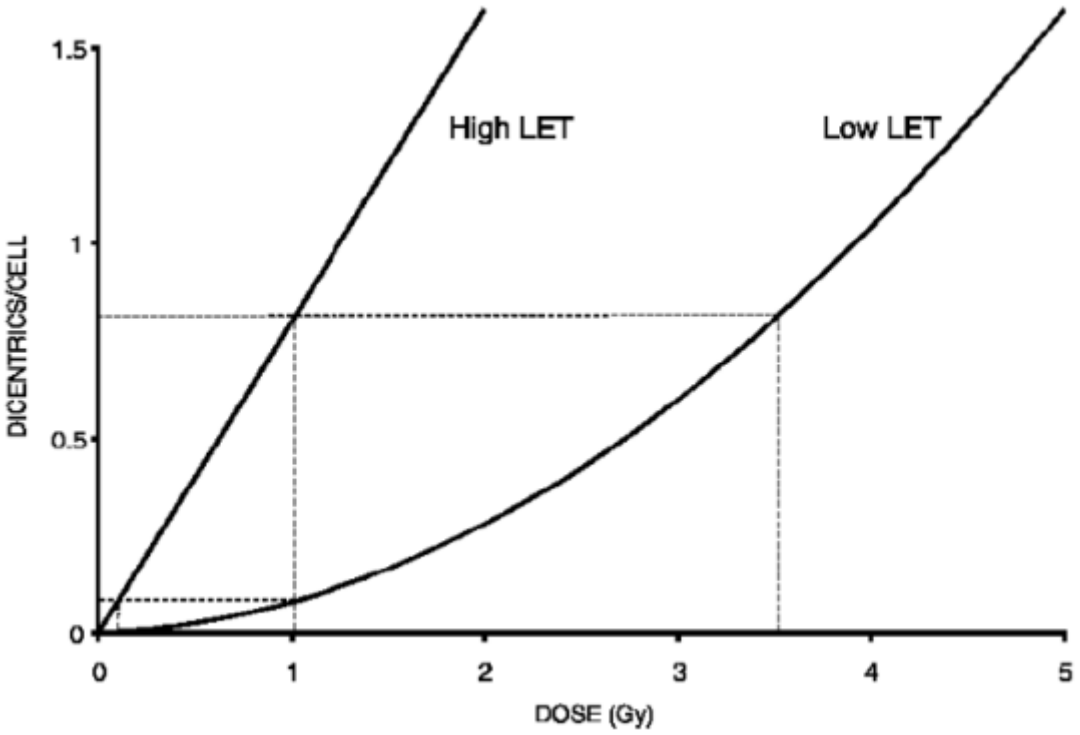

Figure 2.2.5: Linear and linear quadratic dose-response curve [11].

with high-LET radiation, such as neutrons, the probability that one particle causes enough damage to create a chromosome aberration is the same for both high and

low doses, therefore the dose-response curve is fitted by a linear equation:

$$Y = c + \alpha D \tag{2.2.5}$$

where α is a fitted parameter and C is the control value of chromosome mutations. For low-LET radiation, such as photons, the yields (Y) of damages are related to dose (D) by a second-degree polynomial (linear-quadratic) curve:

$$Y = c + \beta D + \gamma D^2 \tag{2.2.6}$$

where C is the control value of CA or micronuclei and β and γ are fitted parameters. The shape of this curve can be attributed to the nature of low-LET radiation. In the case of small doses, the chance of two particles entering the same nucleus is minute, thus chromosome aberrations are caused, very infrequently, by lone particles. As the dose rises, the amount of particles passing through a single nucleus also rises, as well as the amount of radiation-induced chromosome aberrations[20]. In the case of gamma radiation, the shape of the low-LET dose-response curve may also be influenced by how photons ionize matter. The photoelectric and Compton effects cause more expansive ionization clusters, instead of singular tracks.

The equations discussed above (2.2.5 and 2.2.6) are very practical and easy to use, but they imply an unchanging linear (or quadratic) trend of the dose-reponse curves. Unfortunately, for higher doses (several greys or more), the curves do indeed change [2]. This is due to the fact, that above a certain higher dose, most chromosomes in the irradiated cell group have already been damaged, therefore there isn't much room for more alterations. The increase of chromosome aberrations begins to slow down, causing the curve to flatten, creating the saturated versions of equations 2.2.5 and 2.2.6:

$$Y = (Y_{max} - Y_0) \cdot (1 - e^{-\alpha D}) + c \tag{2.2.7}$$

$$Y = (Y_{max} - Y_0) \cdot (1 - e^{-\beta D + \gamma D^2}) + c \tag{2.2.8}$$

where: C - the control value of chromosome aberrations, Y_{max} - the maximum possible amount of chromosome aberrations within one cell (in most cases Y_{max}=1) and α, β, γ - fitted parameters.

Below are graphs illustrating the difference between standard and saturated calibration curves. These particular curves were made with the following parameters: $\alpha = 0.354, \beta = 0.0119, \gamma = 0.0557, Y_0 = 0.0005, Y_{max} = 1$.

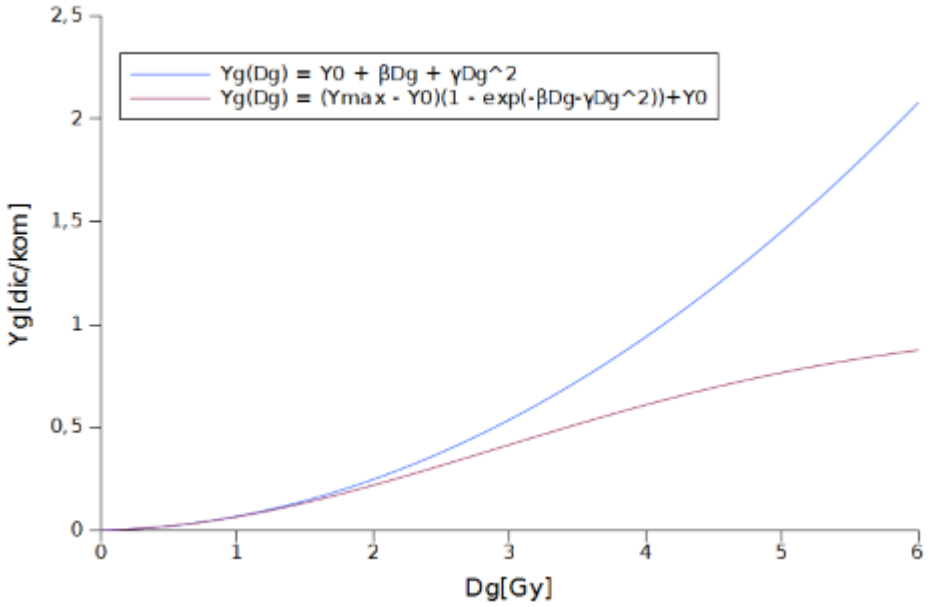

Figure 2.2.6: Calibration curves for gamma radiation

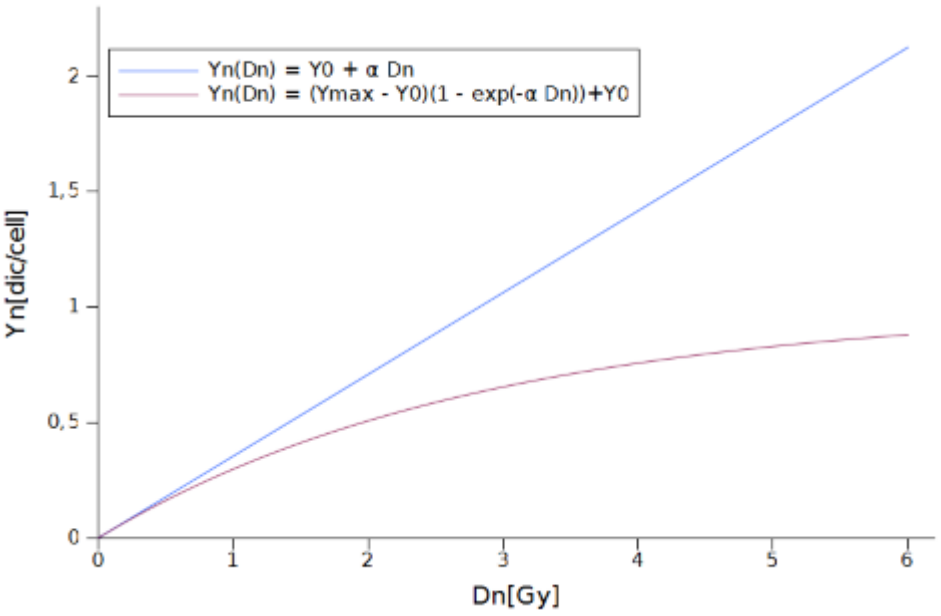

Figure 2.2.7: Calibration curves for neutron radiation

2.2.4 Mixed n+γ field dosimetry

The above description of absorbed dose assessment is more than adequate in the case of exposure to a single type of radiation. It is not, however, sufficient when dealing with mixed radiation, such as the n+γ field.

As mentioned before, neutrons and gamma photons have a very different biological effectiveness. Both the severity and mechanisms of ionization and excitation influence the number of chromosome aberrations induced by each component radi-

ation. Determining how much of the total dose is gamma and neutron radiation is crucial for providing prognostic advice and/or planning treatment of exposed individuals [18]. When scoring chromosome mutations, it is impossible to differentiate between those induced by gamma photons and those induced by neutrons therefore cytogenetic biodosimetry methods by themselves are not enough to assess the absorbed dose. To calculate the two component mutation frequencies we must assume that the total aberration frequency is the sum of the gamma and neutron frequencies caused by the component radiations. There are several statistical methods that can be employed to determine the damage done by each radiation, but the neutron to gamma dose ratio is necessary. If that information is not available, it is possible to approximate it using a prior probability distribution [11][34].

3 | Method

3.1 Background

3.1.1 Introduction

There are a number of statistical methods that can be used to estimate the absorbed doses of mixed radiation components, each has its advantages and limitations. The method employed in this thesis is the Monte Carlo technique and it will be discussed later in this chapter. First, several other theoretical points must be addressed.

3.1.2 Classical methods

Component doses of mixed radiation are most commonly calculated using the iterative method, which can be employed in cases where the neutron to gamma absorbed dose ratio is known:

$$\rho = \frac{D_n}{D_g} \tag{3.1.1}$$

The essence of the iterative method is repetition. In each iteration, the absorbed doses and aberration frequencies of gamma and neutron radiation are re-estimated using information acquired in the previous step. Below is a short outline of the process [11][18]:

1. At first, all aberrations are assumed to be induced by neutron radiation. the neutron absorbed dose (D_n) can be calculated using the total number of aberrations (Y_{total}) and a modified version of equation (2.2.5) :

$$D_n = \frac{Y_{total} - c}{a} \tag{3.1.2}$$

2. Next, equation (3.1.3) is used to calculate the gamma dose (D_g) and equation (2.2.6) to calculate the gamma induced aberration frequency.

$$D_g = \frac{D_n}{\rho} \tag{3.1.3}$$

3. With the assumption that $Y_{total} = Y_n + Y_g$, neutron induced aberration frequency can be estimated:

$$Y_n = Y_{total} - Y_g \tag{3.1.4}$$

4. Y_n is then used to calculate the new value of D_n. The process continues, repeating steps 2 to 4 until a stable result is reached.

The iterative method, recommended by the International Atomic Energy Agency, is a widely known and used technique of assessing mixed-radiation doses [18][32]. It is simple and, with a sufficient amount of iterations, very accurate. Its major disadvantage is that reaching the final result requires a substantial amount of repetitions. As a consequence, the calculations can be very lengthy.

It is possible to implement some modifications to create the analytical version of the iterative method. Again, we assume that $Y_{total} = Y_n + Y_g$, therefore we can express the total dicentric frequency as:

$$Y_{total} = c + \alpha D_n + \beta D_g + \gamma D_g^2 \tag{3.1.5}$$

The variable ρ, which can vary from zero to infinity, is replaced with θ, normalized to the range of <0,1> [2][35].

$$\theta = \frac{D_g}{D_g + D_n} = \frac{1}{\rho + 1} \tag{3.1.6}$$

The parameter θ represents the how much of the total absorbed dose was gamma radiation.

The benefit of modifying the iterative method is shortening the time required to reach a stable result. Instead of completing a number of steps in each iteration, only two variables need to be calculated. The analytical solution can be achieved using equations 3.1.5 and 3.1.6:

$$\begin{cases} D_n(\theta) = \dfrac{1-\theta}{\theta} D_g(\theta) \\ D_g(\theta) = \dfrac{\sqrt{(\alpha\frac{1-\theta}{\theta} + \beta)^2 + 4\gamma(Y_{total} - c)} - (\alpha\frac{1-\theta}{\theta} + \beta)}{2\gamma} \end{cases} \tag{3.1.7}$$

The analytical method is accurate and less time-consuming than the iterative method. The main set-back for both of these techniques is that neither of them can be used if the gamma-to-neutron ratio is not known.

3.1.3 Quasi-Bayesian method

In most accidental exposures to a mixed neutron-gamma field, the exact composition of the radiation is not known. In these cases, θ can be given by a prior function (discussed in section 3.1.4). The quasi-Bayesian method, also called the enhanced classical method, builds on elements of Bayesian statistics as well as on the techniques mentioned in the previous subsection. Equations 3.1.7 are modified

to create probability distributions [2]:

$$\begin{cases} \theta_g(D_g) = \dfrac{D_g}{D_g + \frac{1}{\alpha}(Y_{total} - c - \beta D_g - \gamma D_g^2)} \\ \theta_n(D_n) = \dfrac{\sqrt{\beta^2 - 4\gamma(c + \alpha D_n - Y_{total})} - \beta}{\sqrt{\beta^2 - 4\gamma(c + \alpha D_n - Y_{total})} - \beta + 2\gamma D_n} \end{cases} \tag{3.1.8}$$

Because the exact value of θ is unavailable, two types of θ are calculated, one for neutrons radiation and one for gamma radiation. After changing the variables, the probability distribution of the dose is expressed as [2][18]:

$$p(\theta) = p(\theta_x(D_x))\theta'_x(D_x) \equiv const \cdot P(D_x) \tag{3.1.9}$$

where x=$\{g, n\}$ and p(θ) is a prior function.

Ultimately, the dose is equal to the maximum of the probability distribution, that can be determined via:

$$\frac{dP(D_x)}{dD_x} = 0 \tag{3.1.10}$$

3.1.4 Prior functions

A prior distribution is a probability density function (PDF) that allows us to estimate the most likely value of the observed parameter, in this case θ [2]. Selecting a prior can be approached in two ways, depending on the current state of knowledge, or degree of uncertainty, about the radiation incident in question [13].

The first approach is finding a *non-informative* prior, also called an objective, vague or reference distribution. Choosing this type of prior attempts to remove subjectivity by behaving as though there is minimal, or a complete absence of, pre-existing information about the parameter [13][36]. The simplified Beta distribution is an example of a *non-informative* prior, where a very general assumption is made, that the absorbed dose was half neutrons, half gamma photons:

$$p(\theta) = \theta - \theta^2 \tag{3.1.11}$$

The second is finding an *informative* prior. This type of prior is selected based on previous knowledge, experience and/or data. It is a more subjective approach, but incorporating such information into a data analysis can provide a more precise result [13]. An example of an informative prior is the Gaussian distribution:

$$p(\theta) = \frac{1}{\sqrt{2\pi}\sigma_\theta} exp\left[-\frac{(\theta - \hat{\theta})^2}{2{\sigma_\theta}^2}\right] \tag{3.1.12}$$

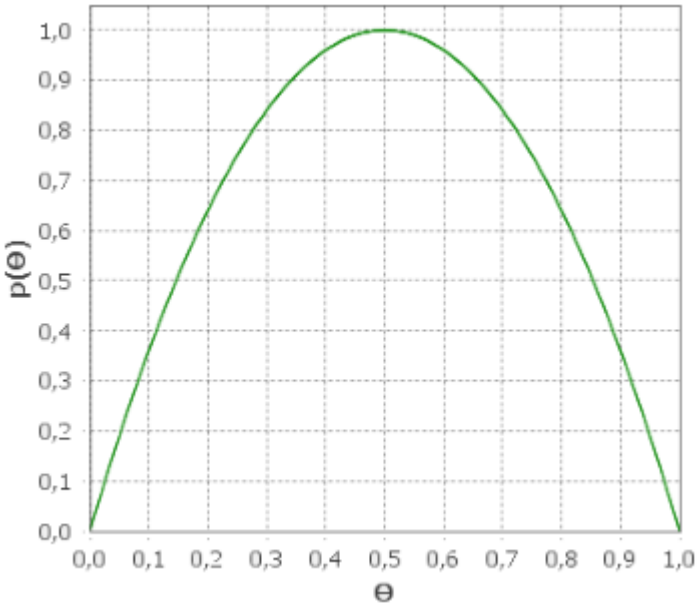

Figure 3.1.1: Simplified Beta distribution

where θ is the unknown parameter, $\hat{\theta}$ is its expected value and σ_θ its standard deviation. Below are two examples of the Gaussian function with the same $\hat{\theta}$ but a different σ_θ.

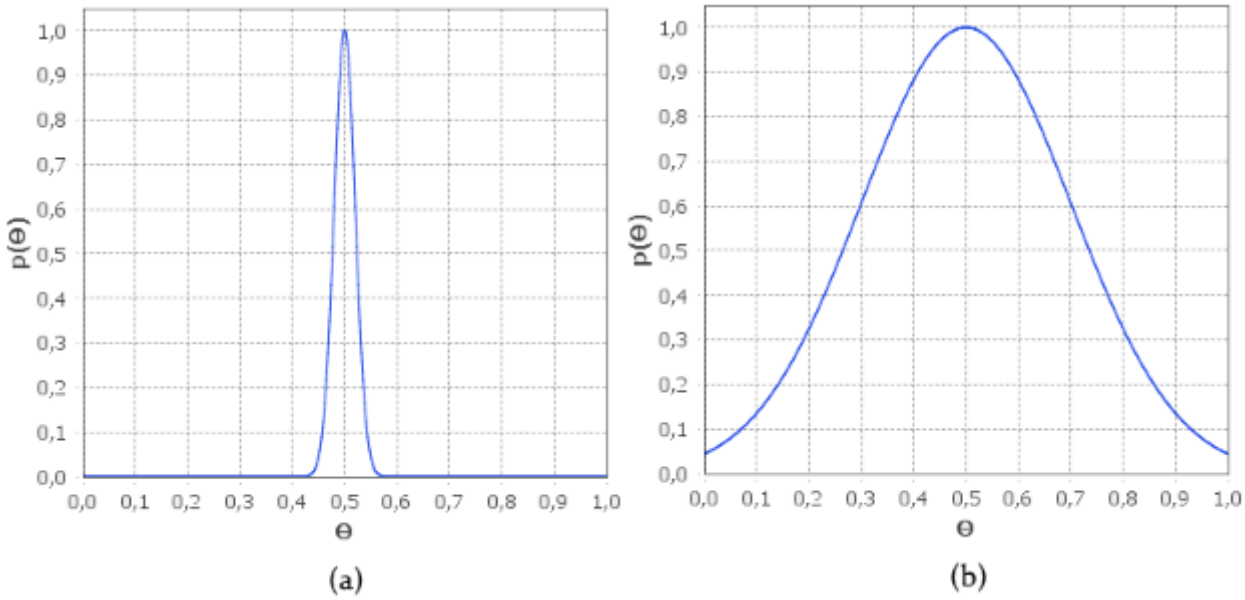

Figure 3.1.2: Gaussian distribution: (a) $\hat{\theta} = 0.5, \sigma_\theta = 0.02$; (b) $\hat{\theta} = 0.5, \sigma_\theta = 0.2$

It's important to note, that not only the expected value of θ can be changed, but also its standard deviation. As illustrated in figure 3.1.2, even the Gaussian distribution, a prior used in the most common cases as an *informative* prior, can be manipulated to resemble the simplified Beta prior, a *non-informative* prior.

3.2 Monte Carlo approach

3.2.1 Introduction

The Monte Carlo (MC) methods are a class of computing algorithms that rely on repeated random sampling as a way of statistically evaluating mathematical functions. This technique is very versatile and is used in a broad spectrum of professions, for example in engineering, finance, manufacturing or insurance. Modern-day Monte Carlo techniques began to emerge and gain popularity in the 1940s, thanks to Fermi, von Neumann, Ulam and Metropolis, among others, who tried to use random sampling as a new approach to solving physics problems [46].

3.2.2 Algorithm

The particular variation of the MC technique used in this thesis is a combination of the classical iterative and the enhanced classical (the quasi-Bayesian) methods. It requires a dedicated computer program that implements the algorithm outlined in figure 3.2.1 [2].

This program has two major loops, the outer loop, repeated over K=500 iterations, where each iteration is a single complete simulation, and the inner loop that repeats over w=1000 cells and contains the core of the algorithm. At the start of the program, the user is prompted to provide some necessary initial information (taken from experiments or measurements), the assumed dicentric count ($y_f = Y_{total}$) and parameters for the calibration curves:

$$\begin{cases} Y_n(D_n) = c + \alpha D_n \\ Y_g(D_g) = c + \beta D_g + \gamma D_g^2 \end{cases} \tag{3.2.1}$$

Before beginning the calculations, the user must chose one of two options, to either use an exact θ or use a probability distribution to approximate its value. This decision depends on the available knowledge about the θ, the gamma-to-total dose ratio.

Within a single iteration of the inner loop, a cell is randomized from the w cells. If the option of using priors was chosen, then a Monte Carlo randomization helps estimate θ. In short [2]:

1. Two values are randomized: θ_j, a temporary value of θ, from the range of [0,1] and p_j from [0,p_{max}] (p_{max} is the maximum possible value of the chosen prior p(θ))

2. Step 1 is repeated until p_j is smaller than or equal to $p(\theta_j)$, the value of the prior in θ_j

If an exact *theta* was given by the user, this step is omitted.

To decide whether the chosen cell was altered by a neutron or by a gamma photon, an additional variable, ξ, is randomized from [0,1] and then compared to θ ($\xi \neq \theta$). If is it bigger than θ, then the damage was caused by neutrons (1 is added to u_n), otherwise the damage came from gamma radiation (1 is added to u_g). The absorbed dose is then calculated using the below equation:

$$D_x = f(u_x) \approx const_x \cdot u_x \tag{3.2.2}$$

where u_x is the amount of dicentrics induced by a specific radiation and x=$\{g, n\}$. The values of $const_g$ and $const_n$ are calculated during the calibration of the program by comparing its results to real data (discussed in 4.1). Equations 3.2.1 are then used to evaluate the aberrations frequency. The inner loop repeats until the total aberration frequency ($Y_g + Y_n$) is no longer smaller than y_f. The doses and aberration frequencies are calculated K time and averaged out [2].

The *stochastic* (random) approach of the Monte Carlo method has a few advantages when compared to other methods [37][2]:

- Statistical analysis - this type of method leaves room for various types of statistical tests, for example a type of "damage time line" can be created or different distributions of cell parameters can be obtained. It is possible to study correlations between different variables.
- Graphical results - the Monte Carlo method generates data in a form that can be represented graphically.
- Probabilistic results - the algorithm provides results as well as how likely they are.

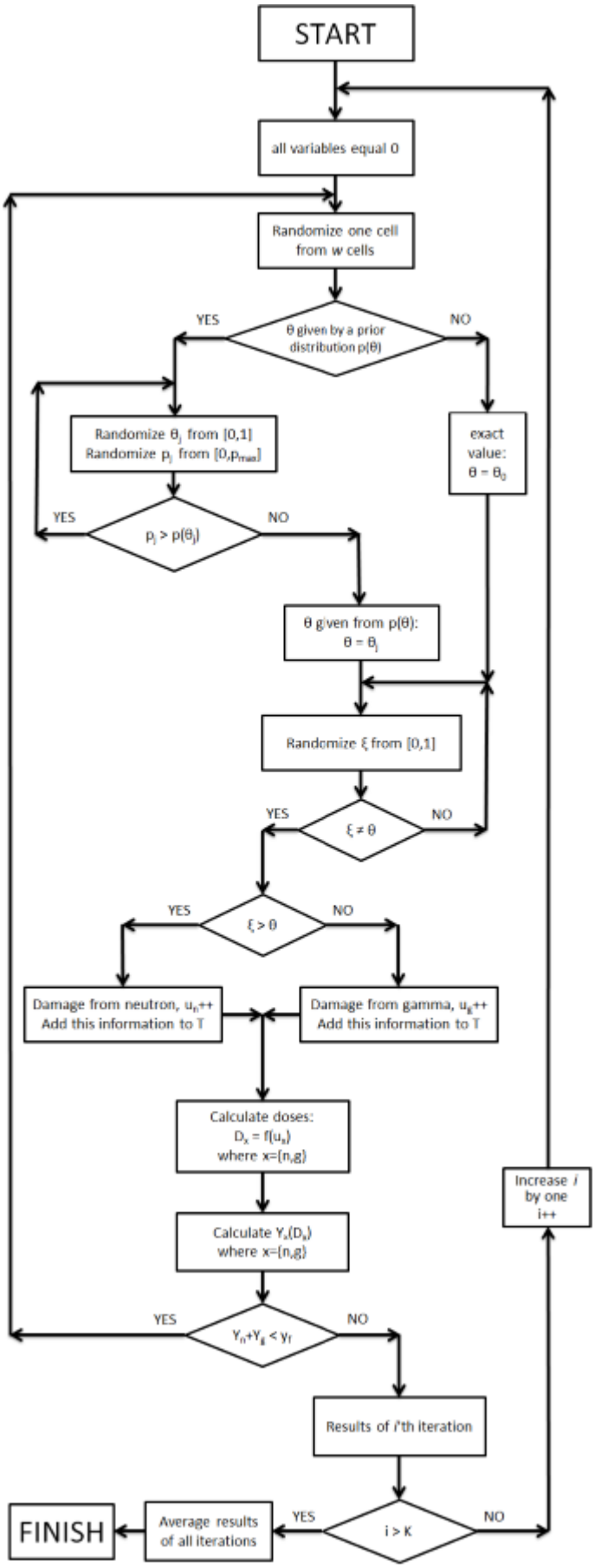

Figure 3.2.1: The Monte Carlo algorithm [2]

3.2.3 Priors

In this Monte Carlo simulation there are eight priors to choose from, depending on the current state of knowledge about the radiation incident.

- Informative Priors
  - The Gaussian distribution

    In the most common cases of accidental irradiation, the Gaussian distribution is used as a prior function. This function is perfectly symmetrical. Both the expected value and the standard deviation can be modified to match the particular situation that is being dealt with.

$$p(\theta) = \frac{1}{\sqrt{2\pi}\sigma_\theta} exp\left[-\frac{(\theta-\hat{\theta})^2}{2{\sigma_\theta}^2}\right] \tag{3.2.3}$$

    where $\hat{\theta}$ is the expected value of θ and σ_θ is the standard deviation.

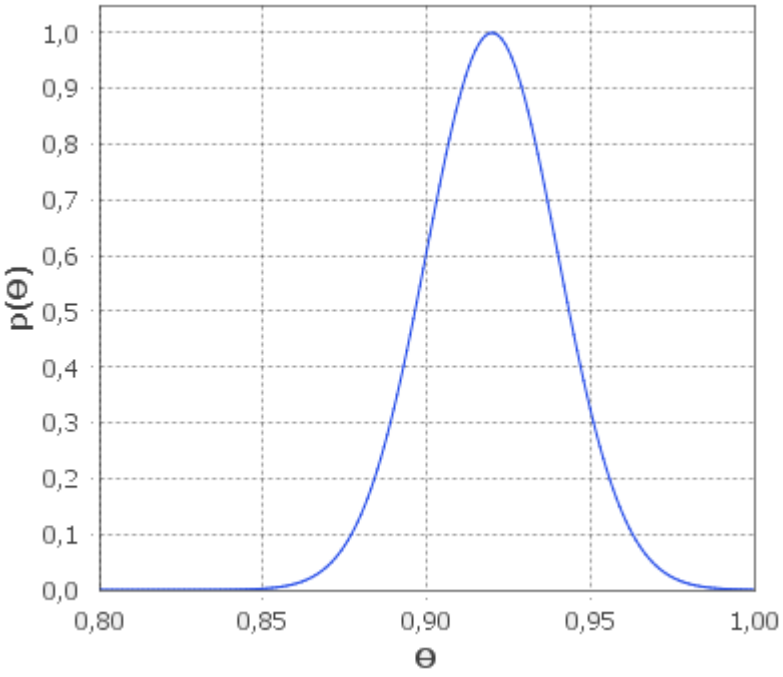

Figure 3.2.2: Gauss distribution: $\hat{\theta} = 0.92$, $\sigma_\theta = 0.02$

  - The scaled Gaussian distribution

    The scaled version of the Gaussian distribution, with normalized values [0,1], can also be used, but $\theta \pm \sigma_\theta$ must be transformed into $\rho \pm \sigma_\rho$, where $\rho = \frac{1}{\theta} - 1$. Figure 3.2.3 compares the standard Gauss and the scaled Gauss.

$$p(\theta) = \frac{1}{\sqrt{2\pi}\sigma_\rho \theta^2} exp\left[\frac{-1}{2\sigma_\rho^2}\left(\left(\frac{1}{\theta} - 1\right) - \hat{\rho}\right)\right] \tag{3.2.4}$$

where $\hat{\rho}$ is the expected value of ρ and σ_ρ is the standard deviation.

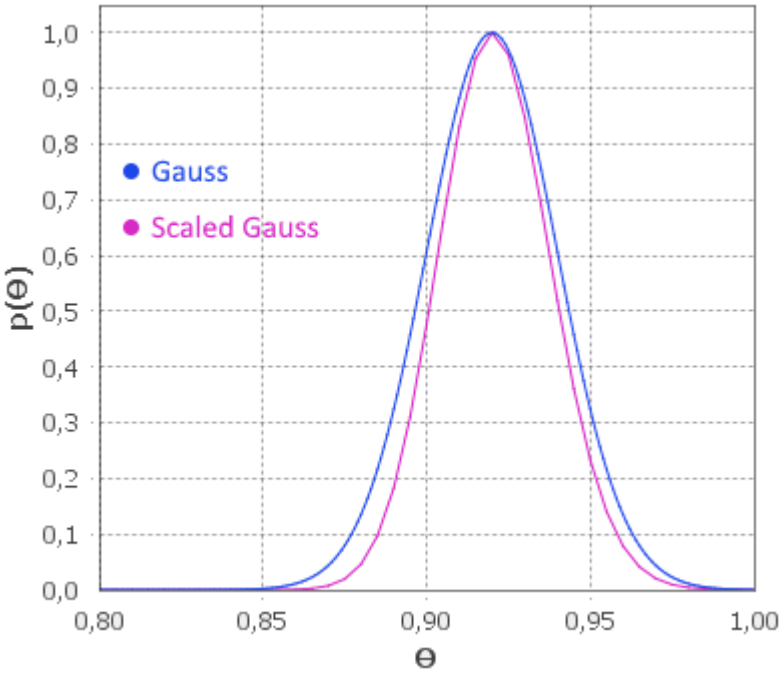

Figure 3.2.3: Scaled Gaussian distribution: $\hat{\rho} = 0.086$, $\sigma_\rho = 0.02$

– The Beta distribution

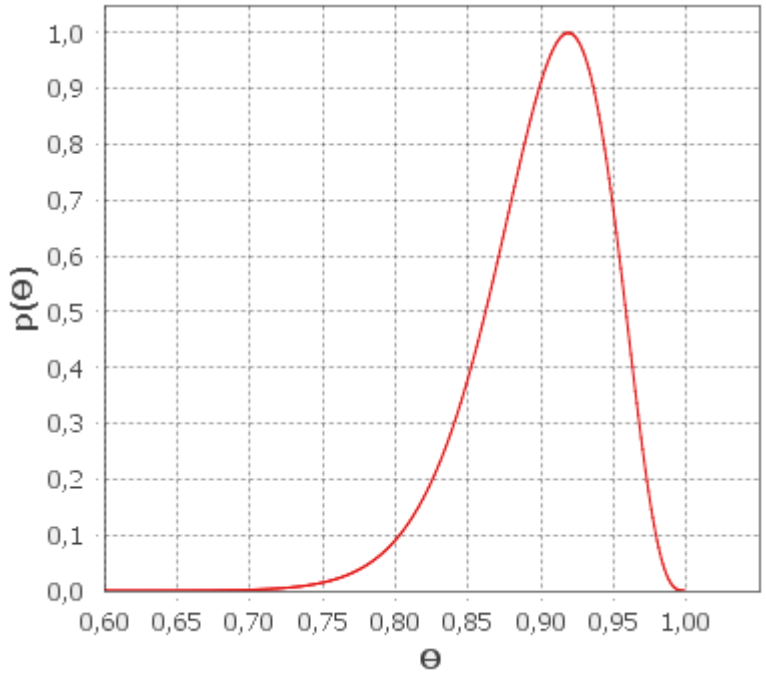

Figure 3.2.4: Beta distribution: a = 41.8, b = 4.6

The Beta distribution is not a symmetrical function, which may make it a counter-intuitive choice for a prior, but it can be used when dealing with critical accidents, where there may have been more neutrons in

the radiation than expected. The shape parameters can be modified to achieve the desired maximum.

$$p(\theta) = \frac{\Gamma(a+b)}{\Gamma(a)\Gamma(b)}\theta^{a-1}(1-\theta)^{b-1} \tag{3.2.5}$$

where a and b are distribution shape parameters (where a,b>0) and Γ is the gamma function.

- Uninformative Priors
  - The simplified Beta distribution

    This distribution is used when no information about the incident is available and the assumption can be made that half of the radiation dose was composed of neutrons and half of gamma photons. The simplified Beta is the standard Beta with a = b = 2.

$$p(\theta) = (\theta - \theta^2) \tag{3.2.6}$$

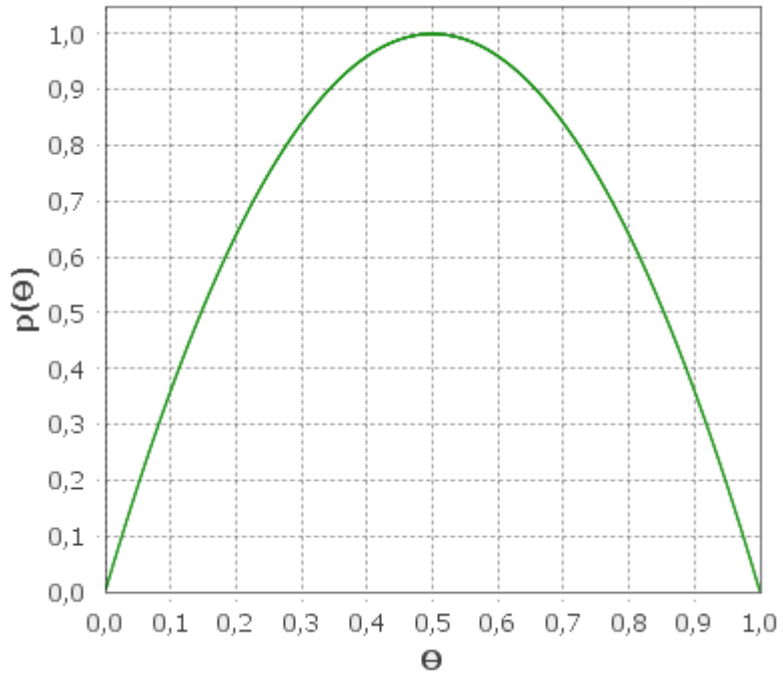

Figure 3.2.5: Simplified Beta distribution

  - The Sigmoidal distribution

    The sigmoidal prior can be used to assess an incident when only gamma photons are expected, but neutrons may occur, for example an uncontrolled fission event. Figure 3.2.6 shows two sigmoidal functions with

different parameters.

$$p(\theta) = \frac{1}{1 + exp(-a\theta + b)} \tag{3.2.7}$$

where a and b are shape parameters.

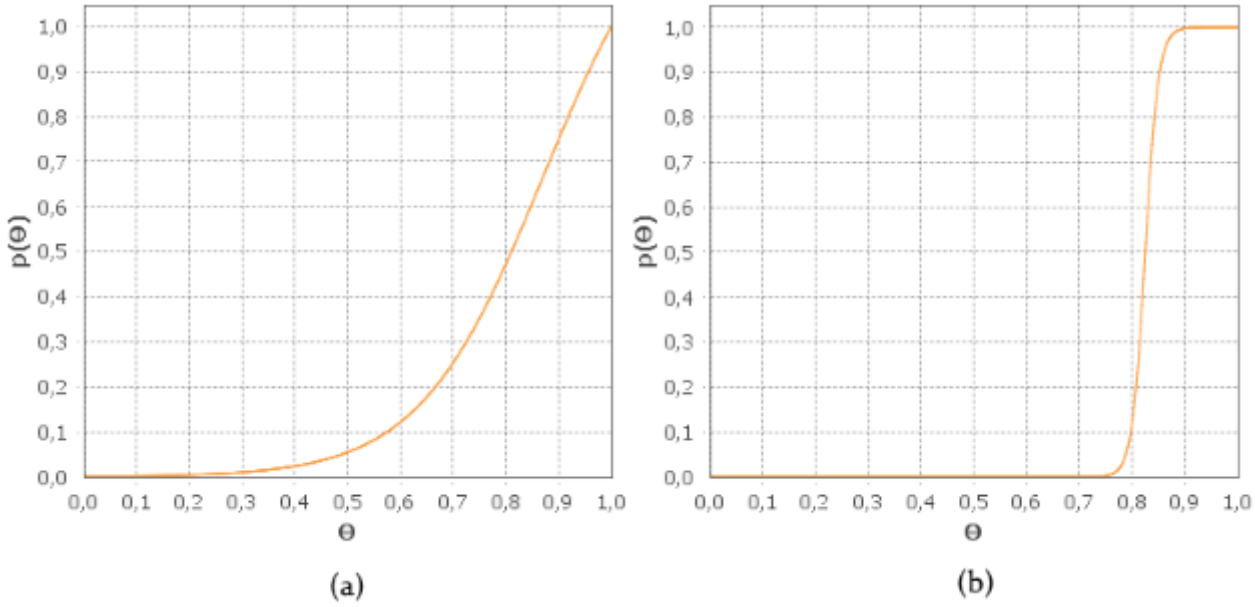

Figure 3.2.6: Sigmoidal distribution: (a) a = 8.5, b = 7.4; (b) a = 80, b = 66

Although both were made with the general assumption that neutrons do not make up more than 20% of the total absorbed dose, figure 3.2.6(b) leaves much less room for mistakes.

– Constant

This is the simplest possible prior. It is used when there is absolutely no information about the irradiation event. It is rarely used because it provides the least accurate results.

$$p(\theta) = const \tag{3.2.8}$$

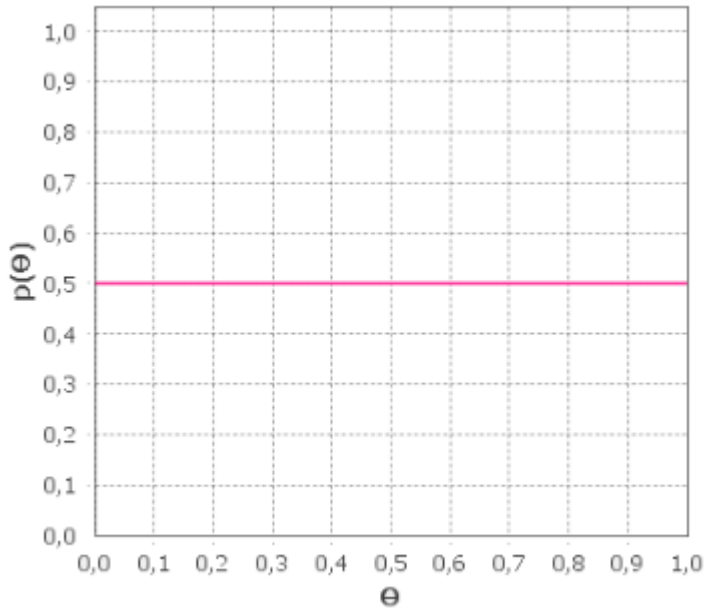

Figure 3.2.7: Constant prior

– Uniform

This distribution is similar to the Constant prior, except that $p(\theta)$ isn't constant throughout the entire range [0,1], but only for a specific interval specified by the user.

$$p(\theta) = \begin{cases} \frac{1}{b-a} & \text{for } a = 1 \\ 0, & \text{otherwise} \end{cases} \tag{3.2.9}$$

where a is the minimum value of θ and b is the maximum value of θ.

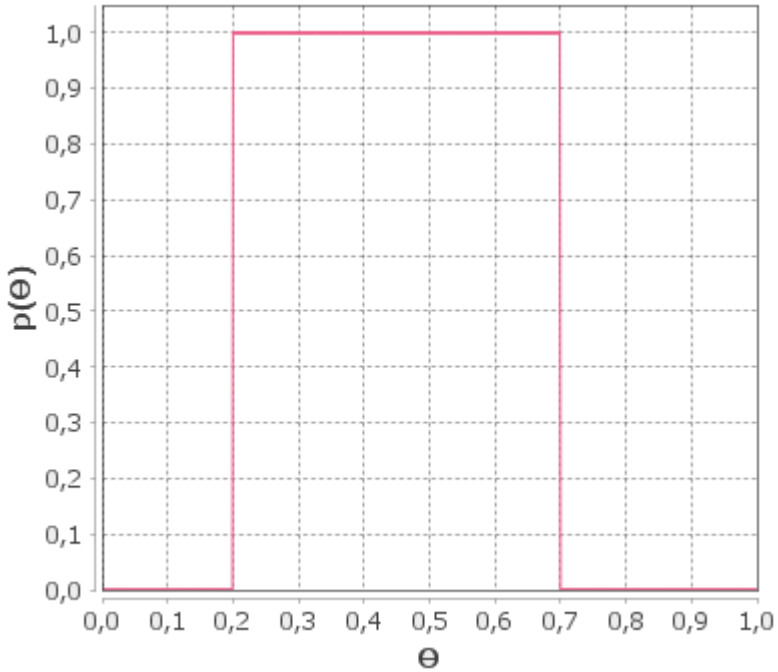

Figure 3.2.8: Uniform distribution: a = 0.2, b = 0.7

The distribution was normalized because the maximum probability for θ is 1.

4 | Results

4.1 Calibration

4.1.1 Introduction

Calibration is an essential part of this program and must be done before any valid results can be generated. The process of properly calibrating is fairly simple. The idea is to determine the appropriate values of $const_g$ and $const_n$ from equation 3.2.2. This is done by modifying the constants until the results generated by the program match the experimental data.

4.1.2 Results

Equation (3.2.2) is an empirical relationship, meaning that it is a correlation based more on observation than on theory. Therefore, the constants $const_g$ and $const_n$ must be assigned a unit. Based on the knowledge that u_x represents the number of dicentrics within the virtual cell group (w=1000), as well as the fact that D_x is expressed in Grays [Gy], the right and left side of the equation can be balanced by assigning $const_g$ and $const_n$ the unit [Gy/dic].

The calibration was done based on blood samples that were irradiated as part of an experiment done in channel H8 of the Maria Reactor, located in Świerk-Otwock. The samples were analysed and assessed through methods of physical dosimetry in the Central Laboratory for Radiological Protection (CLOR). The calibration curves (4.1.1) and (4.1.2) were fitted based on the results of the analysis.

The Maria Reactor generates a specific type of neutron+gamma radiation, where the gamma component of the absorbed dose makes up 92% percent of the total, therefore, the radiation to which the samples were exposed had a θ equal to 0.92 [18].

$$Y_g = (0.0005 \pm 0.0001) + (0.0119 \pm 0.0027)D_g + (0.0557 \pm 0.0016)D_g^2 \qquad (4.1.1)$$

$$Y_n = (0.0005 \pm 0.0001) + (0.354 \pm 0.003)D_n \qquad (4.1.2)$$

Table 4.1.1: Results collected after the irradiation of samples with mixed n+γ radiation ($\theta = 0.92$).

Sample	Total		Gamma		Neutrons	
number	$\mathbf{D_t}$[Gy]	$\mathbf{Y_t}[^{dic}/_{cell}]$	$\mathbf{D_g}$[Gy]	$\mathbf{Y_g}[^{dic}/_{cell}]$	$\mathbf{D_n}$[Gy]	$\mathbf{Y_n}[^{dic}/_{cell}]$
1	0	0.001	0	0.0005	0	0.0005
2	0.25	0.014	0.23	0.006	0.02	0.0075
3	0.5	0.032	0.46	0.018	0.04	0.0145
4	0.75	0.056	0.69	0.035	0.06	0.021
5	0.9	0.076	0.828	0.049	0.072	0.027
6	1	0.086	0.92	0.059	0.08	0.027
7	1.5	0.165	1.38	0.123	0.12	0.042

At first, it was assumed that the value of $const_g$ is the same as the value of $const_n$. The preliminary estimate of the constant ($const_{g,n} \approx 0.012$) was taken from [2]. In the process of calibrating the algorithm, it was discovered that the program generates more precise results when provided with two different parameters. The difference is minimal, yet significant enough to influence the accuracy of the algorithm. Two different constants suggested possible non-linearity of the D_x formula (eq. 3.2.2), but after a few tests it was found, that linear D_g and D_n with separate constants $const_g$ and $const_n$ produce the best results. Below are the constants, that were determined for each test sample by comparing experimental results with those generated by the program:

Table 4.1.2: Calibration constants for each sample.

	Sample number						
	1	**2**	**3**	**4**	**5**	**6**	**7**
const_g	0.012	0.012	0.0127	0.01255	0.0119	0.01255	0.012
const_n	0.012	0.012	0.0122	0.012	0.0123	0.012	0.012

The final values of the constants were calculated by averaging out the parameters from the above table. Uncertainties are discussed in section 4.4.1.

Table 4.1.3: Final values of the calibration constants.

const_g	$(12.243 \pm 0.128) \times 10^{-3} [^{Gy}/_{dic}]$
const_n	$(12.15 \pm 0.08) \times 10^{-3} [^{Gy}/_{dic}]$

4.2 Program

4.2.1 Introduction

The aim of this dissertation is to test the effectiveness of Monte Carlo statistics in assessing absorbed doses of mixed neutron-gamma radiation. In order to

do so, a computer program based on Monte Carlo statistics was created. Both the algorithm and the user-friendly graphical interface were written in Java.

4.2.2 Operating the program

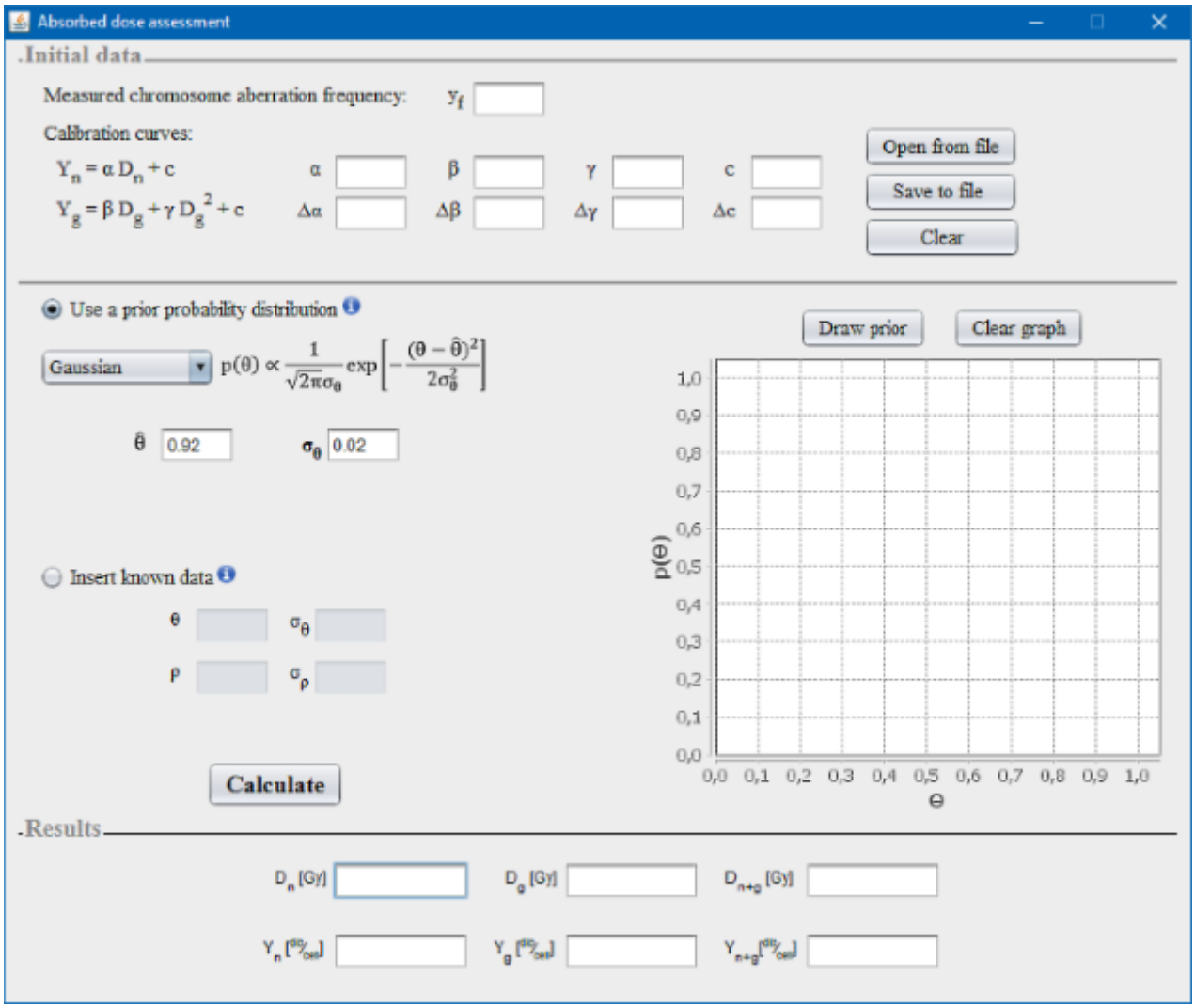

Figure 4.2.1: Graphical User Interface (GUI) of the program written for this thesis.

The final interface of the program is presented in figure 4.2.1.The measured chromosome aberration frequency, y_f, and the calibration curve parameters need to be entered into the program before any calculations can be done. The aberration frequency must be typed in, but the parameters can be either written in or loaded from a file. They can also be saved to a file for future reference. The user must then choose to either use a prior probability function to estimate theta or to provide the actual value of theta. If the latter option is chosen, it is possible to use the value of ρ (the ratio of neutron dose to gamma dose) instead of θ (the ratio of gamma dose to total dose). If the user decides to use a prior, there are seven functions to choose

from. Depending of the prior, different variables can be modified in order to achieve the desired shape and expected value of θ. It is possible to draw several probability functions on the same graph and save them in the form of a PNG file (as shown in figure 4.2.2).

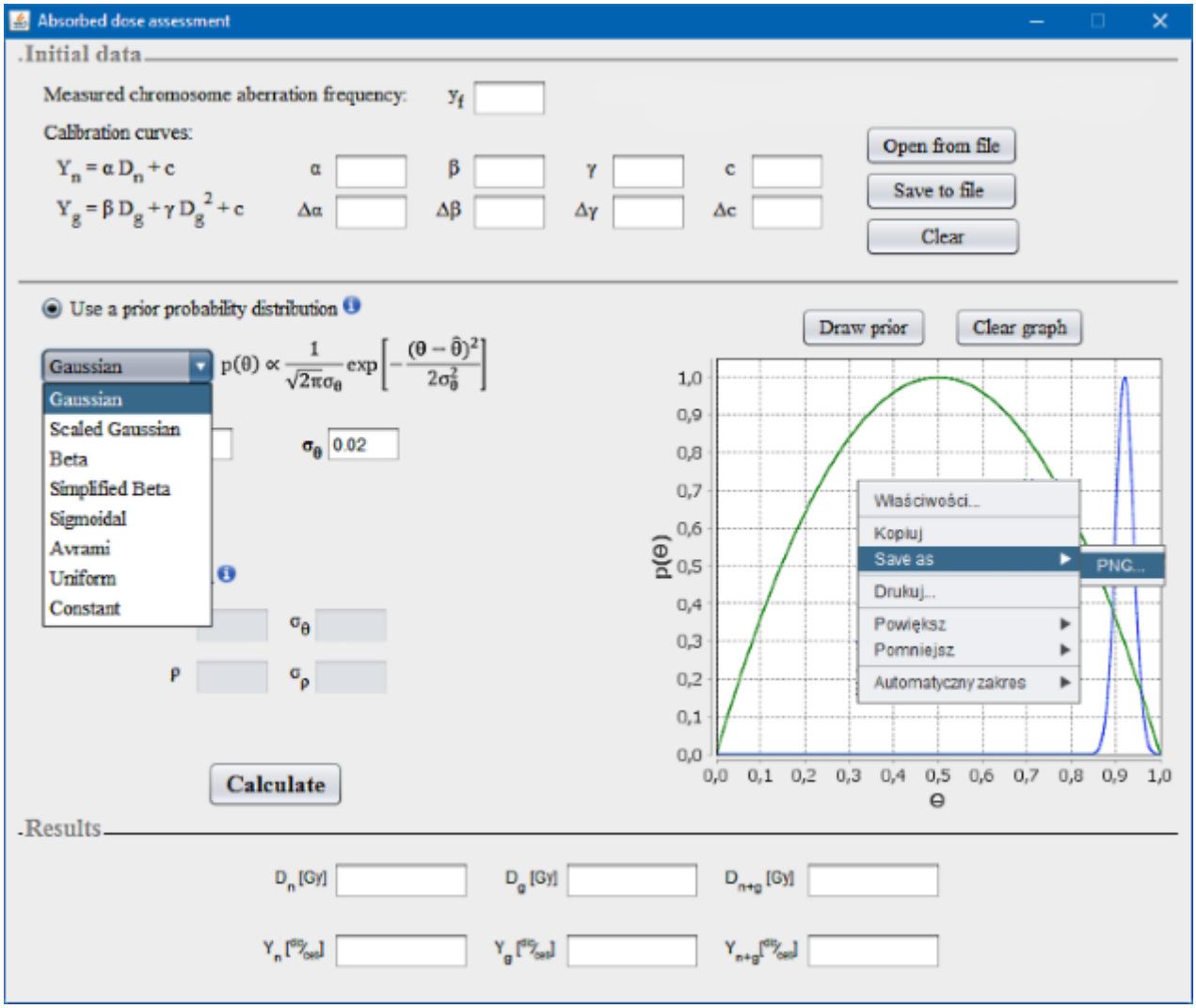

Figure 4.2.2: An example of two priors (Gaussian and simplified Beta) drawn on the same graph.

Once all the necessary information has been filled, the program can assess the absorbed dose. If the aberration frequency y_f is higher than 1, then upon clicking the CALCULATE button, a dialog window will appear on screen with the option to switch from standard to saturated calibration curves. Once the user decides to either keep or change the curves, the program continues its calculations and the results are displayed in the text areas on the bottom of the GUI.

4.2.3 Results

To verify the accuracy of the algorithm, its results have to be compared with experimental data, where the characteristics of radiation beam are known. It is

imperative that the data used for verification is not the same data that was used for calibration. Below are the samples used for the initial testing of the program.

Table 4.2.1: Experimental data used for program verification.

Sample number	$\mathbf{D_t}$[Gy]	$\mathbf{D_g}$[Gy]	$\mathbf{D_n}$[Gy]	$\mathbf{Y_t}[^{\mathbf{dic}}/_{\mathbf{cell}}]$	$\mathbf{Y_g}[^{\mathbf{dic}}/_{\mathbf{cell}}]$	$\mathbf{Y_n}[^{\mathbf{dic}}/_{\mathbf{cell}}]$
1	0.1	0.092	0.008	0.005	0.002	0.003
2	0.85	0.0782	0.068	0.07	-	-
3	2	1.84	0.16	0.27	0.211	0.059

Each blood sample was irradiated in the Maria Reactor in Świerk-Otwock with a mixed n+γ radiation ($\theta = 0.92$). Samples 1 and 3 were collected during the same experiment as the data that was used for calibration, whereas sample 2 was acquired from [35].

Using the Monte Carlo program, the doses and aberration frequencies were assessed in several ways (using standard calibration curves):

1. with no prior: $\theta = 0.92$ and $\sigma_\theta = 0.02$,
2. with the Gaussian prior: $\theta = 0.92$ and $\sigma_\theta = 0.02$,
3. with the scaled Gaussian prior: $\rho = 0.086$, $\sigma_\rho = 0.02$,

To further validate the results, they were compared to doses and aberration frequencies calculated using three other statistical methods: iterative, analytical and Bayesian with a Gaussian prior. For each method: $\theta = 0.92$ and $\sigma_\theta = 0.02$. These calculations were done by a separate program that was created as part of the diploma thesis [38] written by Krzysztof Łukasik. The results are presented in tables 4.2.2 - 4.2.7.

Sample 1:

Table 4.2.2: Sample 1 - Doses.

Method	$\mathbf{D_t}$[Gy]	$\mathbf{D_g}$[Gy]	$\mathbf{D_n}$[Gy]
Monte Carlo			
No prior	0.100 ± 0.059	0.093 ± 0.059	0.008 ± 0.005
Gaussian	0.100 ± 0.061	0.092 ± 0.060	0.008 ± 0.006
Scaled Gaussian	0.100 ± 0.058	0.093 ± 0.058	0.008 ± 0.005
Iterative	-	0.074 ± 0.049	0.006 ± 0.004
Analytical	-	0.094 ± 0.052	0.008 ± 0.004
Bayesian	-	0.093 ± 0.044	0.008 ± 0.004

Table 4.2.3: Sample 1 - Aberration frequencies.

Method	$\mathbf{Y_t}[^{\mathbf{dic}}/_{\mathbf{cell}}]$	$\mathbf{Y_g}[^{\mathbf{dic}}/_{\mathbf{cell}}]$	$\mathbf{Y_n}[^{\mathbf{dic}}/_{\mathbf{cell}}]$
Monte Carlo			
No prior	0.005 ± 0.002	0.002 ± 0.001	0.003 ± 0.002
Gaussian	0.005 ± 0.002	0.002 ± 0.001	0.003 ± 0.002
Scaled Gaussian	0.005 ± 0.002	0.002 ± 0.001	0.003 ± 0.002
Iterative	-	0.002 ± 0.001	0.003 ± 0.002
Analytical	-	0.002 ± 0.001	0.003 ± 0.002
Bayesian	-	0.002 ± 0.001	0.003 ± 0.002

Sample 2:

Table 4.2.4: Sample 2 - Doses.

Method	$\mathbf{D_t}$**[Gy]**	$\mathbf{D_g}$**[Gy]**	$\mathbf{D_n}$**[Gy]**
Monte Carlo			
No prior	0.861 ± 0.084	0.792 ± 0.081	0.068 ± 0.022
Gaussian	0.862 ± 0.086	0.795 ± 0.083	0.067 ± 0.023
Scaled Gaussian	0.864 ± 0.085	0.798 ± 0.082	0.067 ± 0.023
Iterative	-	0.796 ± 0.199	0.069 ± 0.027
Analytical	-	0.798 ± 0.097	0.069 ± 0.021
Bayesian	-	0.798 ± 0.207	0.068 ± 0.023

Table 4.2.5: Sample 2 - Aberration frequencies.

Method	$\mathbf{Y_t}[^{\mathbf{dic}}/_{\mathbf{cell}}]$	$\mathbf{Y_g}[^{\mathbf{dic}}/_{\mathbf{cell}}]$	$\mathbf{Y_n}[^{\mathbf{dic}}/_{\mathbf{cell}}]$
Monte Carlo			
No prior	0.07 ± 0.011	0.045 ± 0.008	0.025 ± 0.008
Gaussian	0.07 ± 0.011	0.046 ± 0.008	0.024 ± 0.008
Scaled Gaussian	0.07 ± 0.011	0.046 ± 0.008	0.024 ± 0.008
Iterative	-	0.045 ± 0.022	0.025 ± 0.010
Analytical	-	0.045 ± 0.010	0.025 ± 0.008
Bayesian	-	0.024 ± 0.008	0.045 ± 0.021

Sample 3:

Table 4.2.6: Sample 3 - Doses.

Method	$\mathbf{D_t}$**[Gy]**	$\mathbf{D_g}$**[Gy]**	$\mathbf{D_n}$**[Gy]**
Monte Carlo			
No prior	2.010 ± 0.079	1.849 ± 0.067	0.160 ± 0.041
Gaussian	2.009 ± 0.078	1.848 ± 0.066	0.161 ± 0.041
Scaled Gaussian	2.012 ± 0.076	1.855 ± 0.065	0.157 ± 0.040
Iterative	-	1.847 ± 0.247	0.161 ± 0.057
Analytical	-	1.850 ± 0.125	0.161 ± 0.054
Bayesian	-	1.850 ± 0.218	0.161 ± 0.041

Table 4.2.7: Sample 3 - Aberration frequencies.

Method	$\mathbf{Y_t}[^{\mathbf{dic}}/_{\mathbf{cell}}]$	$\mathbf{Y_g}[^{\mathbf{dic}}/_{\mathbf{cell}}]$	$\mathbf{Y_n}[^{\mathbf{dic}}/_{\mathbf{cell}}]$
Monte Carlo			
No prior	0.271 ± 0.021	0.213 ± 0.016	0.057 ± 0.015
Gaussian	0.271 ± 0.021	0.213 ± 0.015	0.058 ± 0.015
Scaled Gaussian	0.270 ± 0.021	0.214 ± 0.015	0.056 ± 0.014
Iterative	-	0.213 ± 0.055	0.161 ± 0.057
Analytical	-	0.213 ± 0.029	0.057 ± 0.019
Bayesian	-	0.213 ± 0.049	0.059 ± 0.015

The priors used in these calculations were chosen based on their ability to accurately represent the characteristics of the radiation beam. Because of how well-defined the radiation generated in the Maria Reactor is, it was possible to choose the best fitting probability functions. The results are all within the margin of error, they do not differ from the experimental data by more than 2%. The initial testing of the program shows that the algorithm has been properly implemented and that the calibration was successful.

4.2.4 Additional results

The samples assessed in the previous section in order to test were irradiated by the same source with a moderate dose. Below are three more scenarios that involve higher to extreme doses.

1. Acquired from [39]:
   Post-accident results for a sample exposed to 6 Gy of mixed n+γ radiation with a gamma-to-total absorbed dose ratio of $\theta = 0.61$. A total of 85 dicentrics were scored in 28 cells ($y_f = 3.036$). The radiation field can be described by the following dose-response curves:

$$Y_g = (0.0005 \pm 0.0001) + (0.01420 \pm 0.00001) D_g + (0.07850 \pm 0.00001) D_g^2 \quad (4.2.1)$$

$$Y_n = (0.0005 \pm 0.0001) + (0.834 \pm 0.001) D_n \quad (4.2.2)$$

2. Acquired from [11]:
   An example of a criticality scenario in which 120 dicentrics were scored in 100 cells. The mixed n+γ radiation can be characterized by a θ equal to 0.60. The dose-response curves corresponding to this field are as follows:

$$Y_g = 0.0005 + 0.0164 D_g + 0.0492 D_g^2 \quad (4.2.3)$$

$$Y_n = 0.0005 + 0.832D_n \tag{4.2.4}$$

The results in [11] were calculated using the iterative method:

$\mathbf{D_t}$[Gy]	$\mathbf{D_g}$[Gy]	$\mathbf{D_n}$[Gy]	$\mathbf{Y_t}[^{\mathbf{dic}}/_{\mathbf{cell}}]$	$\mathbf{Y_g}[^{\mathbf{dic}}/_{\mathbf{cell}}]$	$\mathbf{Y_n}[^{\mathbf{dic}}/_{\mathbf{cell}}]$
-	1.82	1.21	-	0.194	1.006

3. Acquired from [32]:
   A criticality scenario involving mixed n+γ radiation with a θ of 0.6, in which 100 dicentrics were scored in 100 cells. The radiation field can be described by the below dose-response curves:

$$Y_g = 0.0005 + 0.014D_g + 0.076D_g^2 \tag{4.2.5}$$

$$Y_n = 0.0005 + 0.83D_n \tag{4.2.6}$$

The results in [32] were calculated using the iterative method:

$\mathbf{D_t}$[Gy]	$\mathbf{D_g}$[Gy]	$\mathbf{D_n}$[Gy]	$\mathbf{Y_t}[^{\mathbf{dic}}/_{\mathbf{cell}}]$	$\mathbf{Y_g}[^{\mathbf{dic}}/_{\mathbf{cell}}]$	$\mathbf{Y_n}[^{\mathbf{dic}}/_{\mathbf{cell}}]$
-	1.45	0.99	-	0.188	0.812

Each sample was assessed using standard calibration curves, both with and without a prior. The probability functions used as well as their parameters were chosen to accurately represent the scenario:

- No prior:
  - sample 1: $\theta = 0.609756$
  - samples 2 and 3: $\theta = 0.60$
- Gaussian prior:
  - sample 1: $\theta = 0.609756$
  - samples 2 and 3: $\theta = 0.60$
- Scaled Gaussian prior:
  - sample 1: $\theta = 0.64$
  - samples 2 and 3: $\theta = 0.67$
- Beta prior:
  - sample 1: a = 60, b = 39.3
  - samples 2 and 3: a = 50, b = 33.4

As was done in section (4.2.3), the results were compared to those calculated using the iterative, analytical and Bayesian methods within the program from [38]. A Gaussian prior was used for the Bayesian method. Tables 4.2.8 - 4.2.13 present the results.

Sample 1:

Table 4.2.8: Sample 1 - Doses.

Method	$\mathbf{D_t}$**[Gy]**	$\mathbf{D_g}$**[Gy]**	$\mathbf{D_n}$**[Gy]**
Monte Carlo			
No prior	6.023 ± 0.194	3.670 ± 0.160	2.354 ± 0.109
Gaussian	6.027 ± 0.198	3.682 ± 0.163	2.345 ± 0.093
Scaled Gaussian	6.040 ± 0.204	3.674 ± 0.168	2.350 ± 0.115
Beta	6.012 ± 0.202	3.636 ± 0.168	2.376 ± 0.113
Iterative	-	3.638 ± 0.921	2.318 ± 0.587
Analytical	-	3.673 ± 0.831	2.351 ± 0.533
Bayesian	-	3.638 ± 0.921	2.318 ± 0.587

Table 4.2.9: Sample 1 - Aberration frequencies.

Method	$\mathbf{Y_t}[^{\mathbf{dic}}/_{\mathbf{cell}}]$	$\mathbf{Y_g}[^{\mathbf{dic}}/_{\mathbf{cell}}]$	$\mathbf{Y_n}[^{\mathbf{dic}}/_{\mathbf{cell}}]$
Monte Carlo			
No prior	3.038 ± 0.127	1.075 ± 0.089	1.963 ± 0.091
Gaussian	3.039 ± 0.130	1.083 ± 0.091	1.956 ± 0.093
Scaled Gaussian	3.038 ± 0.134	1.075 ± 0.094	1.950 ± 0.096
Beta	3.038 ± 0.132	1.056 ± 0.093	1.982 ± 0.094
Iterative	-	1.022 ± 0.512	1.933 ± 0.490
Analytical	-	1.075 ± 0.475	1.960 ± 0.445
Bayesian	-	1.055 ± 0.521	1.933 ± 0.490

Sample 2:

Table 4.2.10: Sample 2 - Doses.

Method	$\mathbf{D_t}$**[Gy]**	$\mathbf{D_g}$**[Gy]**	$\mathbf{D_n}$**[Gy]**
Monte Carlo			
No prior	3.029 ± 0.178	1.817 ± 0.173	1.212 ± 0.041
Gaussian	3.028 ± 0.180	1.816 ± 0.175	1.212 ± 0.041
Scaled Gaussian	3.018 ± 0.180	1.803 ± 0.175	1.215 ± 0.041
Beta	3.025 ± 0.178	1.812 ± 0.175	1.213 ± 0.041
Iterative	-	1.816 ± 0.279	1.21 ± 0.669
Analytical	-	1.816 ± 0.353	1.211 ± 0.684
Bayesian	-	1.814 ± 0.173	1.208 ± 0.308

Table 4.2.11: Sample 2 - Aberration frequencies.

Method	$\mathbf{Y_t}[^{\mathbf{dic}}/_{\mathbf{cell}}]$	$\mathbf{Y_g}[^{\mathbf{dic}}/_{\mathbf{cell}}]$	$\mathbf{Y_n}[^{\mathbf{dic}}/_{\mathbf{cell}}]$
Monte Carlo			
No prior	1.203 ± 0.112	0.194 ± 0.035	1.009 ± 0.106
Gaussian	1.203 ± 0.112	0.194 ± 0.035	1.009 ± 0.107
Scaled Gaussian	1.203 ± 0.112	0.192 ± 0.035	1.011 ± 0.106
Beta	1.203 ± 0.112	0.193 ± 0.035	1.009 ± 0.107
Iterative	-	0.192 ± 0.057	1.008 ± 0.566
Analytical	-	0.193 ± 0.035	1.007 ± 0.578
Bayesian	-	0.192 ± 0.094	1.005 ± 0.275

Sample 3:

Table 4.2.12: Sample 3 - Doses.

Method	$\mathbf{D_t}$[Gy]	$\mathbf{D_g}$[Gy]	$\mathbf{D_n}$[Gy]
Monte Carlo			
No prior	2.449 ± 0.157	1.466 ± 0.151	0.983 ± 0.044
Gaussian	2.453 ± 0.154	1.471 ± 0.148	0.982 ± 0.043
Scaled Gaussian	2.456 ± 0.151	1.475 ± 0.145	0.981 ± 0.041
Beta	2.453 ± 0.154	1.471 ± 0.151	0.982 ± 0.044
Iterative	-	1.467 ± 0.198	0.978 ± 0.122
Analytical	-	1.467 ± 0.267	0.978 ± 0.170
Bayesian	-	1.465 ± 0.408	0.975 ± 0.266

Table 4.2.13: Sample 3 - Aberration frequencies.

Method	$\mathbf{Y_t}[^{\mathbf{dic}}/_{\mathbf{cell}}]$	$\mathbf{Y_g}[^{\mathbf{dic}}/_{\mathbf{cell}}]$	$\mathbf{Y_n}[^{\mathbf{dic}}/_{\mathbf{cell}}]$
Monte Carlo			
No prior	1.003 ± 0.095	0.186 ± 0.038	0.817 ± 0.087
Gaussian	1.003 ± 0.049	0.187 ± 0.033	0.816 ± 0.035
Scaled Gaussian	1.003 ± 0.093	0.188 ± 0.037	0.815 ± 0.086
Beta	1.003 ± 0.049	0.189 ± 0.036	0.814 ± 0.037
Iterative	-	0.184 ± 0.047	0.816 ± 0.102
Analytical	-	0.184 ± 0.063	0.816 ± 0.142
Bayesian	-	0.184 ± 0.096	0.813 ± 0.222

The data shown in tables 4.2.8 - 4.2.13 are very similar and do not vary by more than 3%, which confirms the accuracy of the Monte Carlo algorithm. All of the incidents or scenarios assessed in this subsection, as well as in the previous one, had rather well-defined radiation fields. Calculations could be done with informative

priors or even without priors. The less precise uninformative probability functions (constant, simplified Beta etc.) would have provided inaccurate results. Despite this fact, it is important to note, that there are situations when there is absolutely no information on which to base a dose assessment. In these events, uninformative priors are crucial as they add objectivity and limit speculation.

4.3 Statistical analysis

4.3.1 Introduction

Monte Carlo methods provide the opportunity to carry out various types of statistical tests. In the case of this dissertation, two things are being monitored: the distribution of the doses collected throughout all the iterations and the number of cells that have sustained specific amounts of damages. The data is presented in the form of graphs.

4.3.2 Results

Below are some example results showing the graphical representation of the statistical data. They were generated for several different aberration frequencies y_f.

- y_f=0.05 [$^{dic}/_{cell}$]: figure 4.3.1 and figure 4.3.2
- y_f=0.6 [$^{dic}/_{cell}$]: figure 4.3.3 and figure 4.3.4
- y_f=3.5 [$^{dic}/_{cell}$]: figure 4.3.5 and figure 4.3.6

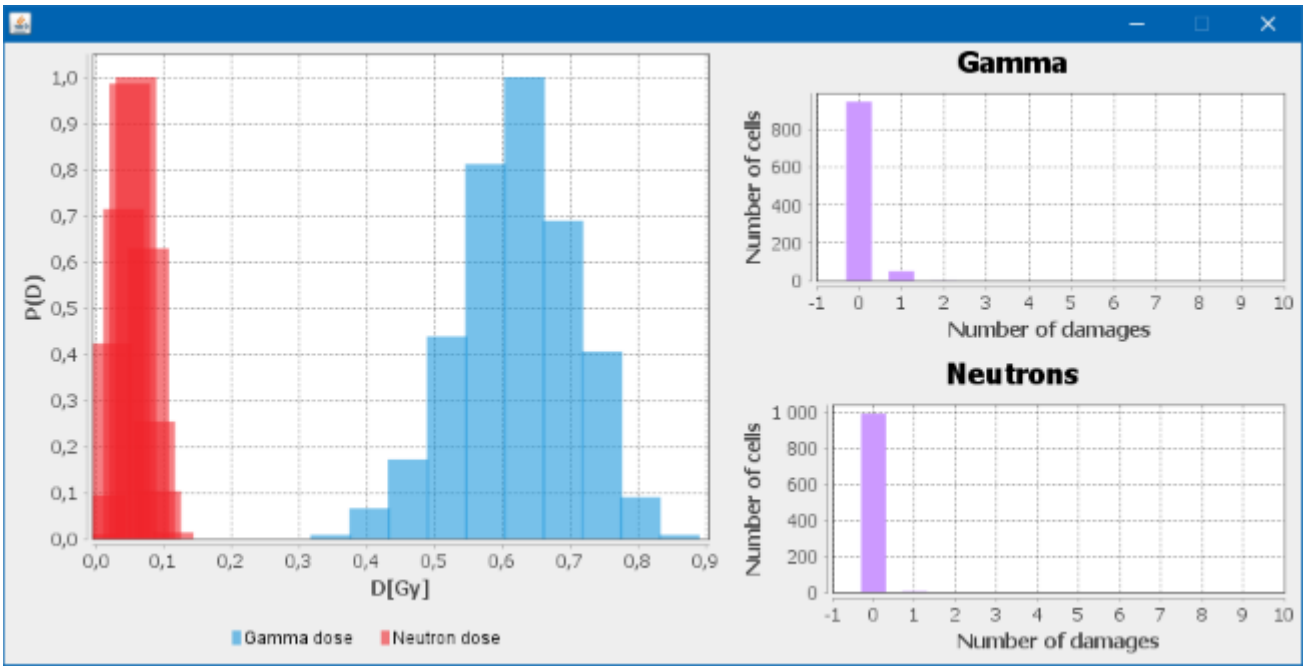

Figure 4.3.1: Results for y_f=0.05 [$^{dic}/_{cell}$], θ=0.92, D_t=0.6 [Gy].

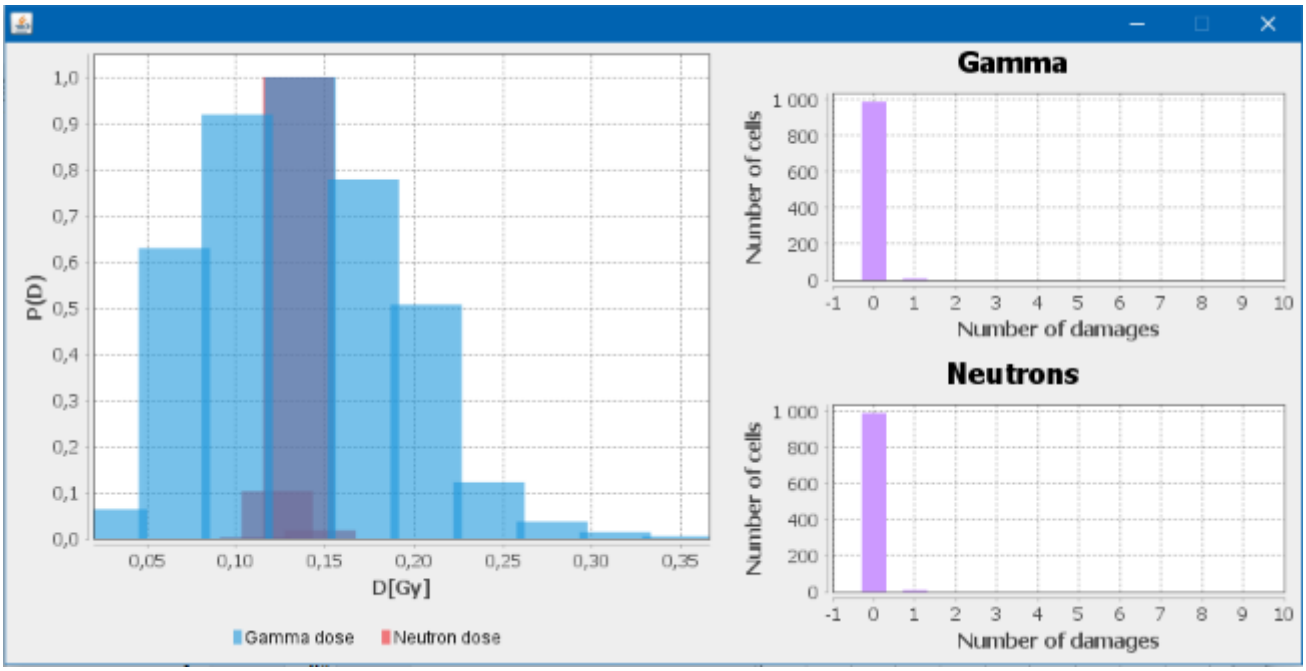

Figure 4.3.2: Results for y_f=0.05 [$^{dic}/_{cell}$], θ=0.5, D_t=0.2 [Gy].

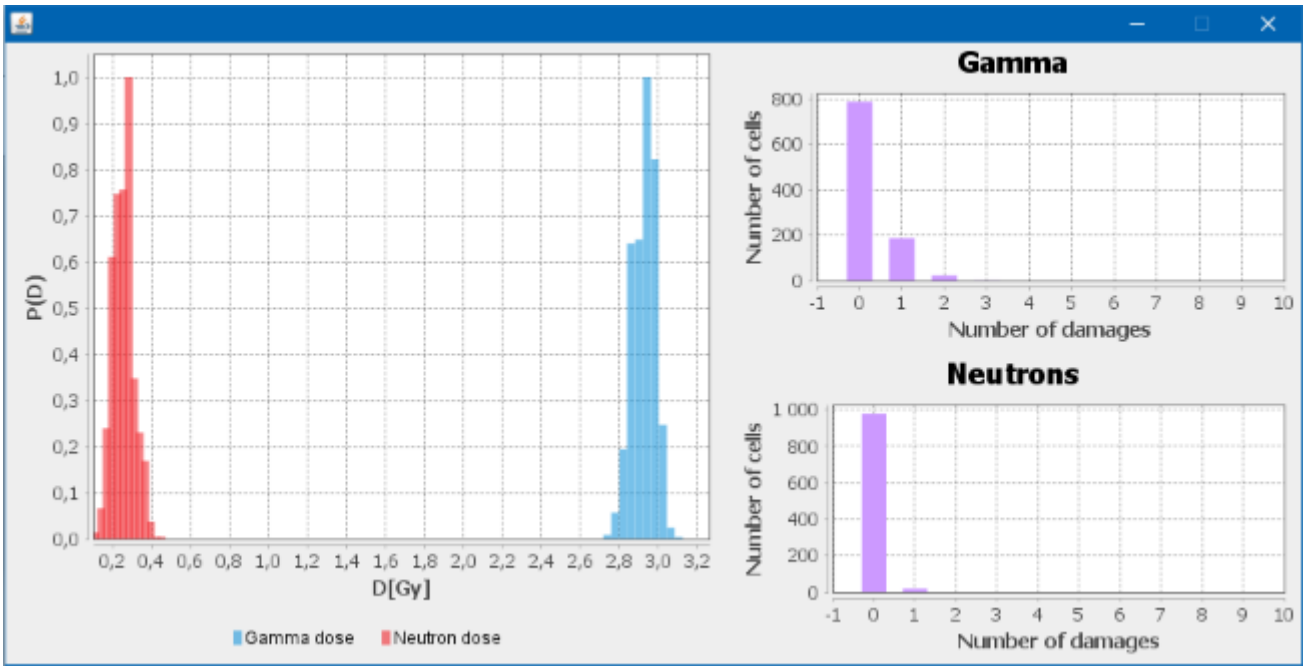

Figure 4.3.3: Results for y_f=0.6 [$^{dic}/_{cell}$], θ=0.92, D_t=3.18 [Gy].

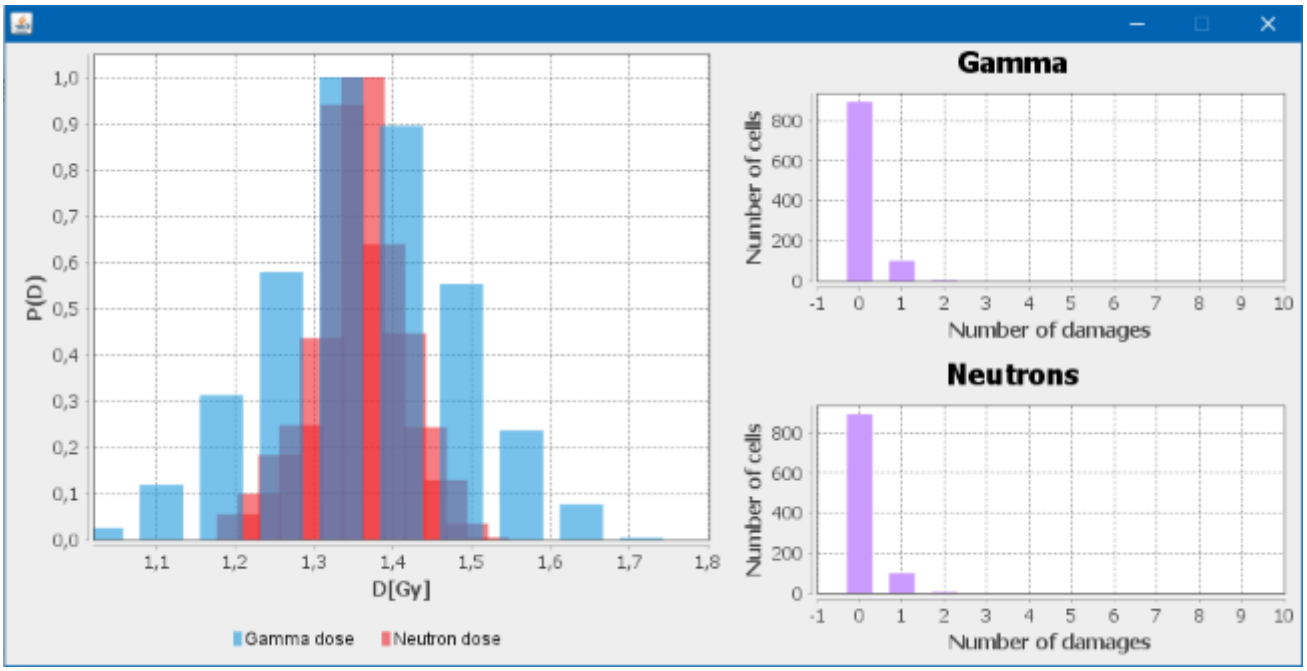

Figure 4.3.4: Results for y_f=0.6 [$^{dic}/_{cell}$], θ=0.5, D_t=2.72 [Gy].

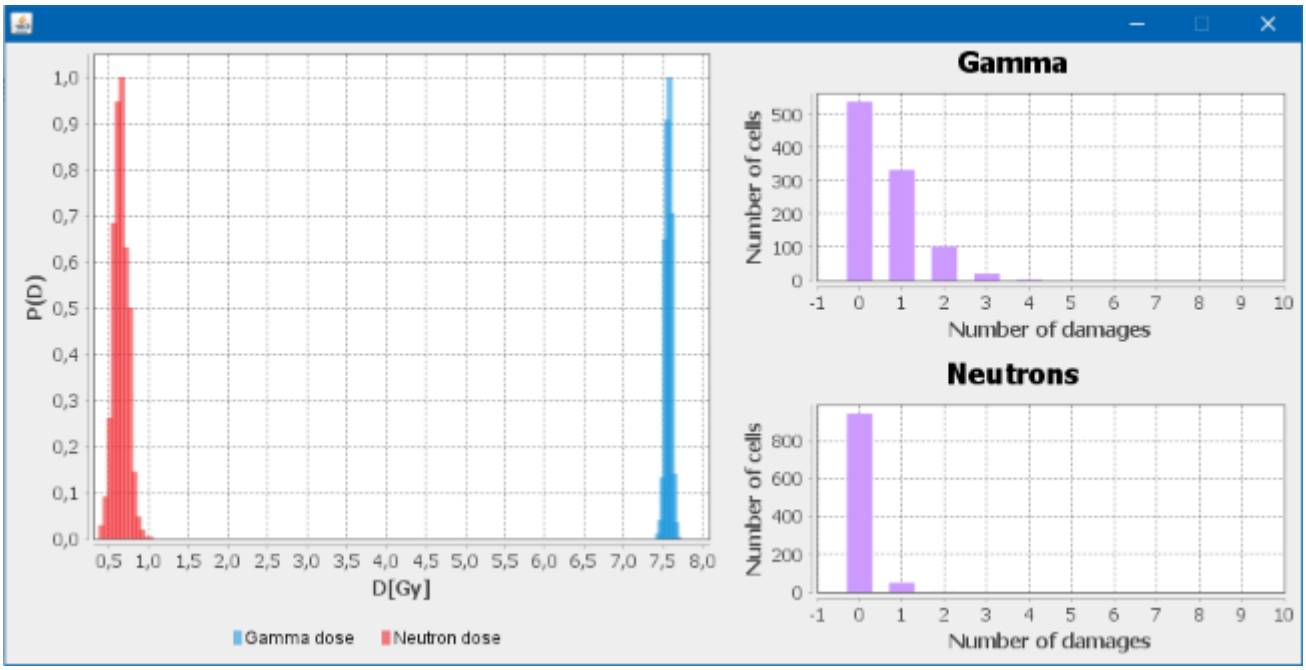

Figure 4.3.5: Results for y_f=3.5 [$^{dic}/_{cell}$], θ=0.92, D_t=8.2 [Gy].

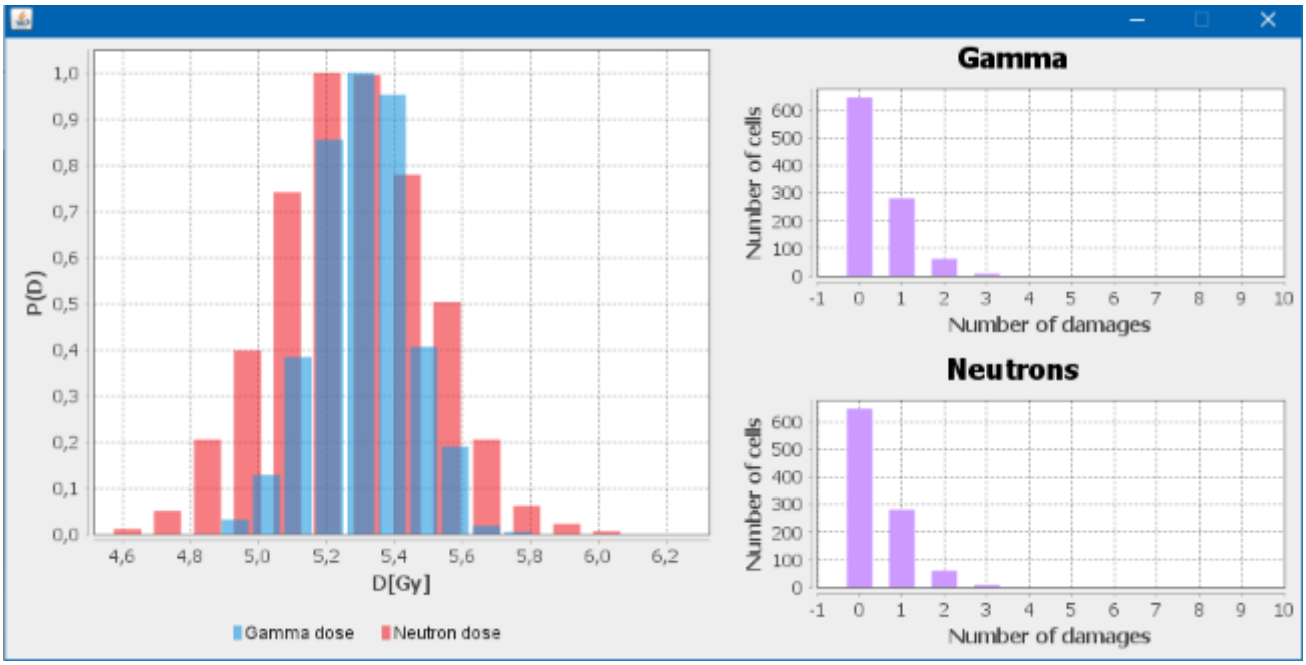

Figure 4.3.6: Results for y_f=3.5 [$^{dic}/_{cell}$], θ=0.5, D_t=10.59 [Gy].

As discussed earlier in this thesis, Monte Carlo statistics rely on random numbers. Because of this, each of the 500 iterations produces a slightly different absorbed dose. The plots on the left are frequency graphs representing how many times a dose appeared throughout all the iterations. The data has been normalized, so the neutron and gamma doses could be shown on the same scale. The expected shape of the frequency graphs is the Gaussian distribution, but because

of the random nature of this method as well as the data collection mechanism, the actual shapes are not exact. For the purpose of this program and calculations, it is assumed that the doses do in fact create a symmetrical Gaussian distribution.

The histograms on the right represent the amount of cells with certain numbers of dicentrics. The number of times cells that are hit by neutrons or gamma photons is a random process that can be modelled as a Poisson distribution. This shape is more visible with higher doses, for example in figure (4.3.4) and (4.3.5). To confirm that the trend continues as the dose rises, results were generated for extreme doses. All of the calculations were done with a θ of 0.5.

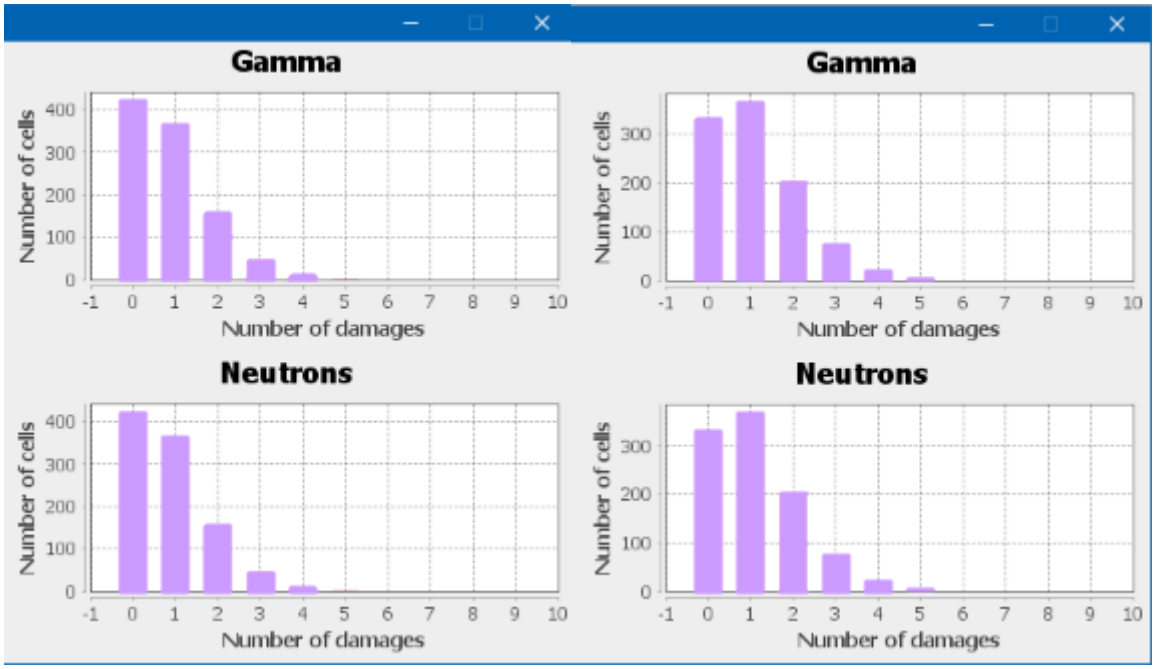

Figure 4.3.7: y_f=10, D=21[Gy]

Figure 4.3.8: y_f=15, D=26.9[Gy]

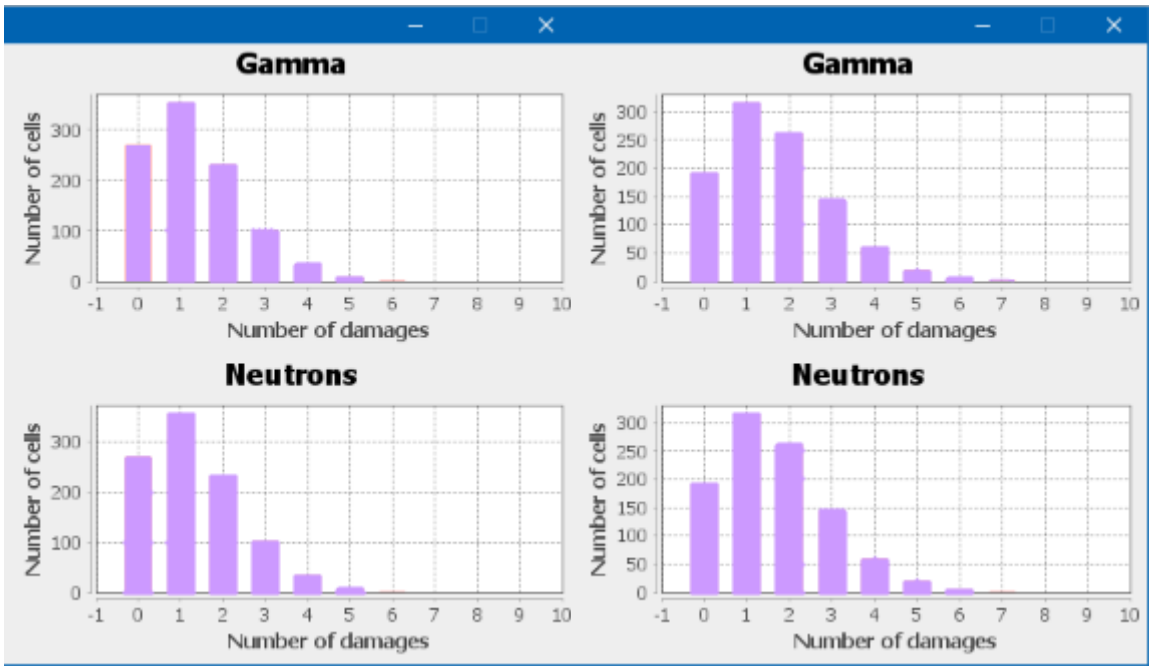

Figure 4.3.9: y_f=20, D=31.9[Gy]

Figure 4.3.10: y_f=30, D=40.3[Gy]

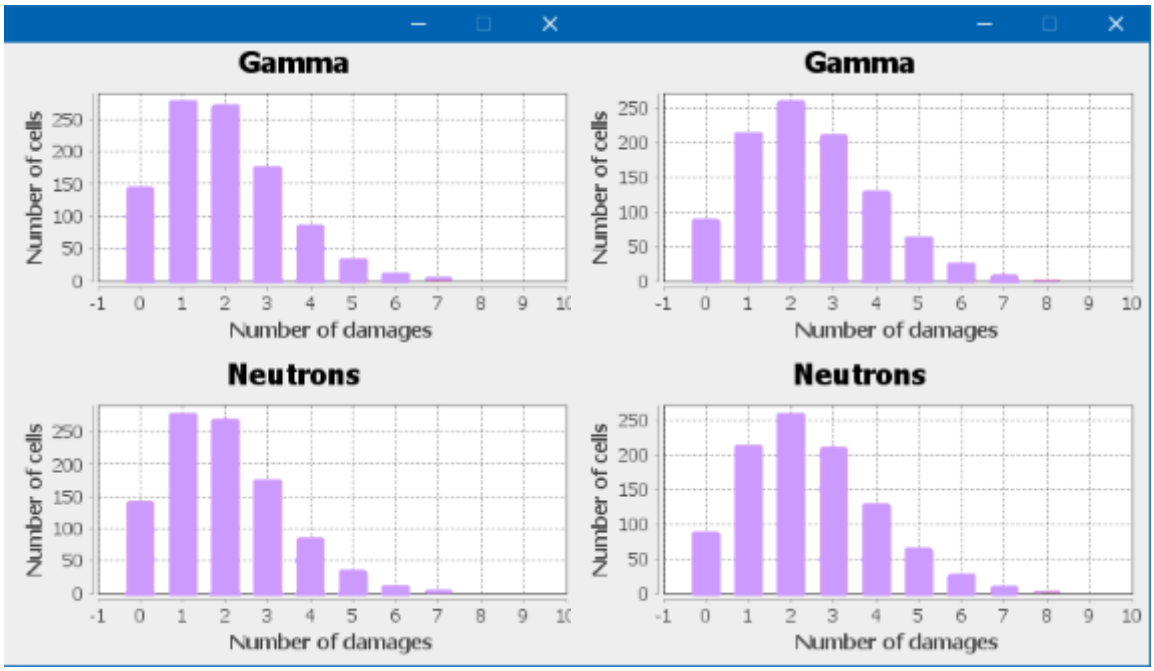

Figure 4.3.11: y_f=40, D=47.4[Gy]

Figure 4.3.12: y_f=60, D=59.4[Gy]

Although the doses are very extreme and rarely occur in practice, they serve the purpose of this thesis very well. The shape of the Poisson distribution is clearly visible on the above histograms. The higher the dose, the wider the shape becomes.

4.4 Uncertainties

4.4.1 Calibration

To account for the variation and dispersion of the constants determined for each sample, uncertainty around the average measurement of the constants was calculated using the standard deviation formula:

$$u(const_{g,n}) = \sqrt{\frac{1}{N}\sum_{i=1}^{N}(x_i - \bar{x})^2} \tag{4.4.1}$$

where: σ - standard deviation, N - the number of samples (the number of constants taken into the average), $\bar{x}$ - the average, x_i - constant value for sample i.

4.4.2 Doses and aberration frequency

The uncertainties of the gamma dose D_g and the neutron dose D_n were calculated using the standard deviation formula 4.4.1. The total dose is the sum of the two component doses, therefore it was calculated using the combined standard uncertainty, which takes into account the uncertainties of each input quantity:

$$u_C(D_t) = \sqrt{\left(\frac{\delta D_t}{\delta D_n}\right)^2 u(D_n)^2 + \left(\frac{\delta D_t}{\delta D_g}\right)^2 u(D_g)^2} \tag{4.4.2}$$

The gamma, neutron and total aberrations frequencies were also determined with the help of the combined standard uncertainty:

$$u_C(Y_g) = \sqrt{\left(\frac{\delta Y_g}{\delta c}\right)^2 \Delta c^2 + \left(\frac{\delta Y_g}{\delta \beta}\right)^2 \Delta\beta^2 + \left(\frac{\delta Y_g}{\delta D_g}\right)^2 u(D_g)^2 + \left(\frac{\delta Y_g}{\delta \gamma}\right)^2 \Delta\gamma^2} \tag{4.4.3}$$

$$u_C(Y_n) = \sqrt{\left(\frac{\delta Y_n}{\delta c}\right)^2 \Delta c^2 + \left(\frac{\delta Y_n}{\delta \alpha}\right)^2 \Delta\alpha^2 + \left(\frac{\delta Y_n}{\delta D_n}\right)^2 u(D_n)^2} \tag{4.4.4}$$

$$u_C(Y_t) = \sqrt{\left(\frac{\delta Y_t}{\delta Y_g}\right)^2 u(Y_g)^2 + \left(\frac{\delta Y_t}{\delta Y_n}\right)^2 u(Y_n)^2} \tag{4.4.5}$$

5 | Discussion

The International Atomic Energy Agency recommends using the classical iterative method for assessing the absorbed dose of mixed radiation [11]. This method has been tried and tested. It has proven to be a trustworthy tool in biological dosimetry, although it is not without fault, as it can't be used if θ, the gamma-to-total absorbed dose ratio, is not precisely known (for example, given by a probability distribution). A Bayesian approach has been introduced to fill this gap and it has also proven accurate. The aim of this thesis was to combine the mechanics and possibilities of Monte Carlo statistics with the functions of the iterative and quasi-Bayesian methods (discussed in 3.1).

The Monte Carlo algorithm was found to give very similar results to the classic iterative method and the quasi-Bayesian method (subsections 4.2.3 and 4.2.4). The general algorithm (figure 3.2.1) is straightforward in understanding and implementation. The user has the option of entering a specific θ or estimating its value by choosing one of seven probability functions, both informative and uninformative, with modifiable parameters. An important benefit of using the Monte Carlo method within the algorithm is that the manner in which data is collected leaves room for more than just dose calculation. A number of various statistical tests can be implemented into the code. This specific program examines two statistical aspects of the data, as discussed in section 4.3.

Similarly to the classical method, Monte Carlo has limitations of its own. First off, this statistical method is based around random sampling. As mentioned in 4.3.2, this results in slightly different absorbed doses and aberration frequencies after each iteration. Since these values are then averaged out to get the final results, these too end up varying slightly between each run. The differences are minimal and are all within the margin of error. They do not effect the overall results. The second limitation regards Monte Carlo statistics as well as any other statistical method used for dose assessment. Assessing doses with aberration frequencies of $y_f = 0.001$ [$^{dic}/_{cell}$] and below is disrupted by the "noise" caused by spontaneously occurring aberrations. Absorbed doses with aberration frequencies that low are rarely assessed in practice, but it is important to be aware of the threshold below which the method that is being used does not generate precise results.

Additionally, the graphic representation of one of the statistical tests implemented within the Monte Carlo algorithm (subsection 4.3.2) is limited. While the histogram showing the distribution of dicentrics among cells presents no issues, the graphs illustrating the distribution of doses collected during all of the iterations aren't always symmetrical. It is important to note that the calculations of the neutron dose are more precise, which sometimes results in a very small amount of bars

on the histogram. It is also worth mentioning is that for low values of aberration frequencies, the graph showing the distribution of gamma doses throughout the iterations becomes incoherent. The threshold value below which this occurs varies depending on the calibration curves used and the value of θ. In the case of dose-response curves (4.1.1) and (4.1.2) and θ=0.92, the threshold is y_f=0.03 [$^{dic}/_{cell}$].

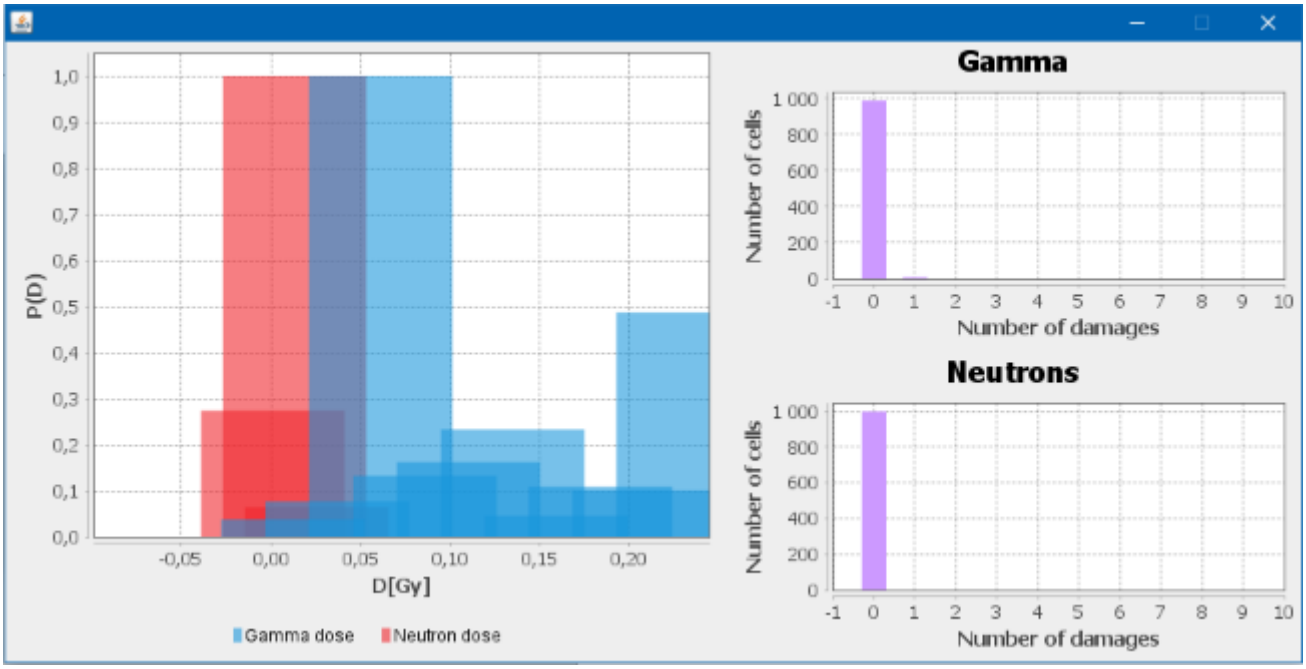

Figure 5.0.1: Graph for y_f=0.007 [$^{dic}/_{cell}$], Gaussian prior θ=0.92, D_t=0.123 [Gy].

Overall, Monte Carlo statistics are a very good alternative to the standard dose assessment methods. The algorithm implementing this method is accurate and the only prominent issues with the program stem from the mechanisms responsible for statistical analysis. These problems do not in any way effect the final results and this part of the code may be improved in the near future. The program can be used within a larger model and applied on a wider scale to analyse radiation risks, assess exposure after a nuclear accident or for emergency planning after a radiological incident.

Bibliography

[1] Iwona Pacyniak, Krzysztof W Fornalski, and Maria Kowalska. *Employment of Bayesian and Monte Carlo methods for biological dose assessment following accidental overexposures of people to nuclear reactor radiation*. Second International Conference on Radiation and Dosimetry in Various Fields of Research, RAD 2014.

[2] Krzysztof Wojciech Fornalski. Alternative statistical methods for cytogenetic radiation biological dosimetry. *arXiv preprint arXiv:1412.2048*, 2014.

[3] Nuclear Power, 2012. http://www.nuclear-power.net/nuclear-power/reactor-physics/atomic-nuclear-physics, Accessed: 2016-05-10.

[4] Jan Pluta. MITJ, Emisja promieniowania jonizującego. http://www.if.pw.edu.pl/~pluta/pl/dyd/mtj/w2013/zrodla1.pdf, Accessed: 2016-05-20.

[5] Krzysztof W. Fornalski and Leon Kananowicz. Modelowanie komputerowe procesu oddziaływania z materią ciężkich cząstek naładowanych, 2004. http://www.fornalski.rootspoland.com/bloch/Bethe-Bloch/index.html, Acessed: 2016-06-03.

[6] Encyclopedia od Health and Safety. Chapter 48 - radiation : Ionizing. http://www.ilocis.org/documents/chpt48e.htm, Accessed: 2016-05-10.

[7] P Rinard. Neutron interactions with matter, chapter 12. *Passive Nondestructive Assay of Nuclear Materials (NUREG/CR-5550/LA-UR-90-732. Prepared by Los Alamos National Laboratory for the Office of Nuclear Regulatory Research. US Nuclear Regulatory Commission, 1991)*, 1991.

[8] Tatjana Jevremovic. *Nuclear principles in engineering*. Springer, 2005.

[9] Norbert Ensslin. The origin of neutron radiation, chapter 11, passive nondestructive assay nuclear materials. Technical report, NUREG/CR-5550, 1991.

[10] Wikipedia. nuclear reactor. https://en.wikipedia.org/wiki/Nuclear_reactor, Accessed:2016-07-25.

[11] International Atomic Energy Agency et al. Cytogenetic dosimetry: applications in preparedness for and response to radiation emergencies. Technical report, International Atomic Energy Agency, 2011.

[12] Myron Pollycove. Nonlinearity of radiation health effects. *Environmental health perspectives*, 106(Suppl 1):363, 1998.

[13] Mark E Glickman and David A van Dyk. Basic bayesian methods. *Topics in Biostatistics*, pages 319–338, 2007.

[14] IAEA. Cytogenetic Analysis for Radiation Dose Assessment. A Manual. *Technical Report Series no. 405*, 2001.

[15] National Research Council. *Assessment of the Scientific Information for the Radiation Exposure Screening and Education Program*. The National Academies Press, Washington, DC, 2005.

[16] IAEA. Retrospective Dosimetry by Translocation Analysis. Lecture. Module 5.

[17] Ademir Amaral. Trends in biological dosimetry: an overview. *Brazilian Archives of Biology and Technology*, 45(SPE):119–124.

[18] Iwona Pacyniak. *Biological assessment of mixed doses of ionizing radiation using Bayesian statistical methods*. Master's thesis, Warsaw University of Technology, 2014. http://www.fornalski.rootspoland.com/pacyniak.pdf, Accessed: 2016-05-20.

[19] Phillip McClean. Variations in chromosome structure: Translocations, 1997.

[20] Iwona Pacyniak. Dozymetria Biologiczna. Cytogenetyczna rekonstrukcja otrzymanej dawki promieniowania jonizującego. 2012, http://www.if.pw.edu.pl/~pluta/pl/dyd/mtj/zal1/pz14/I-Pacyniak.pdf, Accessed: 2016-05-15.

[21] M. Fenech, M. Kirsch-Volders, A. T. Natarajan, and et al. Molecular mechanisms of micronucleus, nucleoplasmic bridge and nuclear bud formation in mammalian and human cells. *Mutagenesis*, 26(1):15–132, 2011.

[22] Stefano Bonassi, Ariana Znaor, Marcello Ceppi, and et al. An increased micronucleus frequency in peripheral blood lymphocytes predicts the risk of cancer in humans. *Carcinogenesis*, 28(3):625–631, 2006.

[23] Dudley T Goodhead. The initial physical damage produced by ionizing radiations. *International journal of radiation biology*, 56(5):623–634. Taylor & Francis, 1989.

[24] IAEA. Radiation protection in diagnostic and interventional radiology. L3: Biological effects of ionizing radiation. IAEA Training Material on Radiation Protection in Diagnostic and Interventional Radiology.

[25] IAEA. Radiation Protection in Radiotherapy, Part 3 - Biological Effects. IAEA Training Material on Radiation Protection in Diagnostic and Interventional Radiology.

[26] IAEA. Dose-Effect Curves; Deterministic and Stochastic Effects of Radiation. Module IX.

[27] National Council for Radiation Protection and Measurements (NCRP). Principles and Application of Collective Dose in Radiation Protection. Technical Report 121, 1995.

[28] PJ Mountford and DH Temperton. Recommendations of the international commission on radiological protection (icrp) 1990. *European Journal of Nuclear Medicine and Molecular Imaging*, 19(2). Springer, 1992.

[29] Steven M Carr. The millisievert and milligray as measures of radiation dose and exposure, 2015. https://www.mun.ca/biology/scarr/Radiation_definitions.html, Accessed: 2016-08-08.

[30] Willian F Blakely. Chapter 6: Early-phase biological dosimetry. *Medical consequences of radiological and nuclear weapons*, 140(12):101–125. Department of the Army, 2012.

[31] Anna Giovanetti, Antonella Scura, and Giorgia Aversa. *Biological Dosimetry: How to measure the absorbed dose in different scenarios*. ENEA, 2012.

[32] M Szłuińska, AA Edwards, and DC Lloyd. *Statistical methods for biological dosimetry*. Health Protection Agency, Radiation Protection Division, 2005.

[33] IAEA. Premature Chromosome Condensation (PCC) Analysis. Lecture. Module 6.

[34] Biological Dosimetry IAEA. Chromosomal aberration analysis for dose assessment. *Tech. Reports Series*, (260), 1986.

[35] Iwona Pacyniak, Krzysztof W Fornalski, and Maria Kowalska. Alternatywne metody obliczania dawek pochłoniętych w biologicznej dozymetrii promieniowania mieszanego n+ γ. *Postępy Fizyki*, 66(1-4):13–22, 2015.

[36] Mário AT Figueiredo. Lecture notes on bayesian estimation and classification. *Instituto de Telecomunicacoes-Instituto Superior Tecnico*, 2004.

[37] Monte Carlo Simulation. 2016, http://www.palisade.com/risk/monte_carlo_simulation.asp, Accessed: 2016-08-01.

[38] Krzysztof Łukasik. *Zastosowanie statystyki bayesowskiej jako narzędzie w dozymetrii biologicznej*. Bachelor's thesis, Warsaw University of Technology, 2016.

[39] RS Brame and PG Groer. Bayesian methods for chromosome dosimetry following a criticality accident. *Radiation protection dosimetry*, 104(1):61–63, 2003.

[40] AJF Griffiths, JH Miller, DT Suzuki, and et al. *An introduction to genetic analysis*. W.H. Freeman and Company, 7 edition, 2000. Deletions. http://www.ncbi.nlm.nih.gov/books/NBK21904/, Accessed: 2016-05-16.

[41] Bradly G Wouters. Cell death after irradiation: how, when and why cells die. *Basic Clinical Radiobiology. 4th ed. London: Hodder Education*, pages 27–40, 2009.

[42] Instytut Fizyki UMCS. Promieniotwórczość w środowisku naturalnym. http://www.radioaktywnosc.umcs.lublin.pl/?id=3, Acessed: 2016-07-20.

[43] David P Landau and Kurt Binder. *A guide to Monte Carlo simulations in statistical physics*. Cambridge university press, 2014.